MAR 1 0 1980

Dan 830-H-15 NAS1.60: 1581

NASA Technical Paper 1581

COMPLETED ORIGINAL

Comparison of Analytical and Flight Test Identified Aerodynamic Derivatives for a Tandem-Rotor Transport Helicopter

Ward F. Hodge

FEBRUARY 1980

NASA

56

NASA Technical Paper 1581

Comparison of Analytical and Flight Test Identified Aerodynamic Derivatives for a Tandem-Rotor Transport Helicopter

Ward F. Hodge
Langley Research Center
Hampton, Virginia

National Aeronautics
and Space Administration

**Scientific and Technical
Information Office**

1980

SUMMARY

Flight tests were conducted for the purpose of verifying an analytical aerodynamic derivative model of a CH-47 tandem-rotor helicopter at low cruise speeds and transition to hover portions of curved, decelerating landing approach flight paths. The flight testing was performed on a closed loop basis with the stability augmentation system (SAS) of the CH-47 operating, and transient response data were obtained using both manual and computer-generated input maneuvers.

The model verification consisted mainly of comparing the existing analytical derivatives with those identified from the flight data using both extended Kalman filter (EKF) and maximum likelihood estimation (MLE) algorithms, then comparing the measured response time histories with those predicted by each of the three sets of derivatives. The overall evaluation further included verification of the analytical SAS model, as well as investigation of the effects of closed loop flight testing on derivative identification.

The results indicate some amplitude and frequency differences between the measured response time histories and those predicted by the analytical derivatives that vary in magnitude with each test run; these differences appear to be mainly due to inaccurate values for some derivatives. The presence of nonzero trim accelerations in the flight data affected the MLE and EKF identified derivatives so that the time histories predicted from them also differed from the measured ones. With some exceptions the discrepancies are not severe, and the overall agreement between the measured and computed time histories is reasonably good.

The results further indicate no adverse effects attributable to closed loop flight testing, nor any deficiencies in the analytical modeling of the SAS. The use of computer-generated input maneuvers proved to be superior to manual ones and was found to be highly effective in generating transient response data having good modal excitation without exceeding small perturbation amplitude bounds. Subsequent flight testing for other purposes indicated that the problem with nonzero trim accelerations could be largely eliminated by also using the fly-by-wire control system to automatically trim the aircraft prior to initiating a test maneuver.

INTRODUCTION

Avionics research for helicopters has been in progress at the Langley Research Center over the past several years as part of the VTOL approach and landing technology (VALT) program (ref. 1). An NASA/Army/Boeing Vertol CH-47 helicopter served as the basic research aircraft for a comprehensive test program which has as its ultimate goal the development of technology necessary for optimum VTOL short haul transportation in the coming decade. The need for a suitable analytical description of the helicopter dynamics, and the rationale

for selecting a linear perturbation model based on aerodynamic stability and control derivatives, is delineated in reference 2.

The extensive tables of aerodynamic derivatives contained in reference 2 were generated by means of an analytical small perturbation technique, involving detailed equations for the helicopter forces and moments, and cover essentially the entire CH-47 flight regime. Although these derivatives appeared to provide a good representation of the helicopter dynamics, comparison with results obtained from actual flight data remained as an important step in verifying the chosen analytical model. The flight tests described in reference 3 were designed to obtain suitable data for this purpose and, also, to permit identification of aerodynamic derivatives for comparison with the tabulated analytical values. Because landing approach and transition to hover from low cruise speeds of about 60 knots comprise the flight regime of primary interest for the VALT program, flight data for the remainder of the CH-47 operating range were unnecessary and were not obtained.

The actual flight testing and ensuing derivative identification activities were planned and conducted in cooperation with the Structures Laboratory of the U.S. Army Research and Technology Laboratories (USARTL) at the Langley Research Center. A joint effort was undertaken with the objectives being to make the model verification as comprehensive as possible and to provide a basis for evaluating differing methods of identifying aerodynamic derivatives from flight data. Reference 4 contains comparisons of analytical derivatives from reference 2 with those computed by USARTL using an extended Kalman filter (EKF) algorithm and with preliminary values from the maximum likelihood estimator (MLE) employed in the present report.

The primary purpose herein is to document the completed MLE results and to include comparisons of measured transient response time histories with those predicted by each available set of analytical and identified derivative values. The effect of the CH-47 stability augmentation system (SAS) on the derivative identification process was also investigated, as the flight testing was necessarily conducted on a closed loop basis to avoid unstable responses which quickly exceed acceptable small perturbation bounds. This mode of testing further provided the opportunity to verify the analytical model of the SAS given in reference 5. An additional objective of the flight test program was to compare results obtained by using conventional doublet type manual input maneuvers with those from computer-generated inputs, implemented by utilizing the fly-by-wire control system of the test aircraft in conjunction with an onboard computer. (See ref. 4.)

SYMBOLS

A,B,C,K,Z aircraft SAS model matrices (eqs. (10) and (11))

A_1,A_2 control input amplitude coefficients, cm (eq. (21))

b measurement bias vector

d data sample (eq. (23))

F,G	aircraft dynamics system matrices (eq. (4))
f	frequency, Hz
g	acceleration due to gravity, m/sec^2
H,D	aircraft response measurement system matrices (eq. (3))
h_n	digital filter weights (eq. (26))
I_X, I_Z, I_{XZ}	aircraft moments of inertia, kg m^2
J	MLE performance function (eq. (1))
N	number of data samples or digital filter weights
n_x, n_y, n_z	body axis components of aircraft linear acceleration, g units
P,Q,R	roll, pitch, and yaw rates about aircraft body axes, respectively, deg/sec
p,q,r	perturbations in P, Q, and R, respectively, deg/sec
p	MLE parameter identification vector (eq. (2))
R(t)	weighting matrix
S	number of filtered data samples
t	time, sec
U,V,W	body axis components of aircraft linear velocity, m/sec
u,v,w	perturbations in U, V, and W, respectively, m/sec
U	aircraft control input vector
u	perturbation in U (eq. (10))
v	aircraft SAS model state vector (eq. (10))
w	white measurement noise vector (see equation following eq. (5))
X	aircraft state vector
x	perturbation in X (eq. (10))
Y	aircraft output response vector
y	perturbation in Y (fig. 2)
δ_{long}	longitudinal control input, cm

δ_{coll} collective control input, cm

δ_{lat} lateral cyclic control input, cm

δ_{rud} differential control input, cm

$\delta_{\phi,SAS}, \delta_{\theta,SAS}, \delta_{\psi,SAS}$ roll, pitch, and yaw SAS feedback command signals, respectively, cm

κ control input amplitude scale factor (eq. (21))

Φ,Θ roll and pitch attitudes about aircraft body axes, deg

ϕ,θ perturbations in Φ and Θ, deg

φ aircraft stability and control derivatives vector

ω frequency, rad/sec

Subscripts:

c control input or cut-off frequency

f final value

m measured value

i,j,k indices for scalar, vector, or matrix quantities

n index

o initial, trim, or central value

t termination frequency

SAS stability augmentation system

Notation:

E( ) statistical expectation

$( )^{-1}$ matrix inversion

$( )^{T}$ matrix transposition

$(\hat{})$ estimated value

$\Delta( )$ increment

$(\bar{})$ normalized or average value

Abbreviations:

EKF	extended Kalman filter
MLE	maximum likelihood estimator
SAS	stability augmentation system
USARTL	U.S. Army Research and Technology Laboratories
VALT	VTOL approach and landing technology
VTOL	vertical take-off and landing

MAXIMUM LIKELIHOOD ESTIMATOR

The aerodynamic derivative estimates documented in this report were computed by means of the maximum likelihood estimator of reference 6. The mathematical development of the MLE algorithm as used herein is described by equations (1) to (9); and the aerodynamic derivative model employed for the CH-47, by equations (10) to (20).

Algorithm Formulation

The algorithm for implementing the MLE estimator is formulated in the same manner as in reference 7, except for added computational options, and is based on minimizing the error in the perturbation response output of the aircraft in the least squares sense by using a performance function of the form

$$J(p) = \int_{t_o}^{t_f} \left[y_m(t) - \hat{y}(p,t) \right]^T R(t)^{-1} \left[y_m(t) - \hat{y}(p,t) \right] dt$$

where $y_m(t)$ and $\hat{y}(p,t)$ are the measured and estimated output response vectors over a data-gathering period $[t_o, t_f]$, and $R(t)$ is a symmetric, positive-definite weighting matrix. Since the algorithm is developed in discrete form for computational reasons, $J(p)$ is approximated:

$$J(p) \approx \sum_{i=1}^{N} \left[y_{m,i} - \hat{y}(p)_i \right]^T R^{-1} \left[y_{m,i} - \hat{y}(p)_i \right] \qquad (1)$$

which represents N samples of the output error during $[t_o, t_f]$. The corresponding least squares normal equations $\frac{\partial J}{\partial p} = 0$ are then solved for $\hat{p}$, which includes the derivative estimates $\hat{\varphi}$, by means of the differential correction procedure

$$\hat{p}_{j+1} = \hat{p}_j + \Delta\hat{p}_j$$

$$= \hat{p}_j + \left[\sum_{i=1}^{N} \left(\frac{\partial \hat{y}_i}{\partial p}\right)^T \hat{R}^{-1} \left(\frac{\partial \hat{y}_i}{\partial p}\right)\right]^{-1} \left[\sum_{i=1}^{N} \left(\frac{\partial \hat{y}_i}{\partial p}\right)^T \hat{R}^{-1} (y_{m,i} - \hat{y}_i)\right]_j \qquad (2)$$

which is also called a quasilinearization or modified Newton-Raphson minimization technique. (See ref. 6.) As in reference 7, the convergence criteria used was $|\Delta\hat{p}_j| \leq |0.01\,\hat{p}_j|$ simultaneously for all elements of $\hat{p}$.

If the measured control input and output response vectors $u_{m,i}$ and $y_{m,i}$ are assumed to have the forms

$$u_{m,i} = u_i + b_c + w_{c,i}$$

and

$$y_{m,i} = y_i + b + w_i$$

which account for the presence of biases and random white noise, the estimated output $\hat{y}_i$ required in evaluating equation (2) is then modeled as

$$\hat{y}_i = H(p)\ \hat{x}_i + D(p)\ \hat{u}_i + \hat{b} \qquad (3)$$

where the state vector $\hat{x}_i$ is obtained by numerical integration of the aircraft dynamical equations

$$\frac{d}{dt}(\hat{x}_i) = F(p)\ \hat{x}_i + G(p)\ \hat{u}_i \qquad \left(\hat{x}_o = (\hat{x})_{t=0}\right) \qquad (4)$$

and the control input vector $\hat{u}_i$ is estimated from

$$\hat{u}_i = u_{m,i} - \hat{b}_c \tag{5}$$

The weighting matrix R in equation (1) is conventionally taken to have the diagonal form

$$R\delta_{ij} = E\left[w_i w_j\right]^T \qquad \left(\delta_{ij} = \begin{cases} 1 & (i = j) \\ 0 & (i \neq j) \end{cases}\right)$$

where $E[w_i] = 0$ at every sample point. Furthermore, the estimate $\hat{R}$ used in equation (2) is recalculated at each iteration of the differential correction process from the expression

$$\hat{R}\delta_{jk} = \frac{1}{N}\sum_{i=1}^{N}\left(y_{m,i} - \hat{y}_i\right)_j\left(y_{m,i} - \hat{y}_i\right)_k^T \qquad \left(\delta_{jk} = \begin{cases} 1 & (j = k) \\ 0 & (j \neq k) \end{cases}\right) \tag{6}$$

Other than the specific forms of the vectors and matrices, which are defined with the aerodynamic derivative model for the CH-47 in the next section, the remaining quantities to be determined in evaluating equation (2) are the partial derivatives $\partial\hat{y}_i/\partial p$ obtained by differentiating equations (3) and (5):

$$\frac{\partial\hat{y}_i}{\partial p} = H(p)\frac{\partial\hat{x}_i}{\partial p} + \frac{\partial H(p)}{\partial p}\hat{x}_i + \frac{\partial D(p)}{\partial p}\hat{u}_i - D(p)\frac{\partial\hat{b}_c}{\partial b_c} + \frac{\partial\hat{b}}{\partial b} \tag{7}$$

in which $\partial\hat{b}_c/\partial b_c$ and $\partial\hat{b}/\partial b$ (as well as $\partial\hat{x}/\partial x_o$ in eq. (8) below) are equivalent to identity matrices of suitably corresponding dimensions. Since the full rank of the parameter vector $\hat{p} = \left[\hat{\varphi}\,|\,\hat{b}_c\,|\,\hat{b}\,|\,\hat{x}_o\right]^T$ includes the option for estimating the initial state conditions $\hat{x}_o$ as well as the aerodynamic derivatives and biases, the following partitioning of

$$\frac{\partial\hat{y}_i}{\partial p} = \left[\frac{\partial\hat{y}}{\partial\varphi}\,\middle|\,\frac{\partial\hat{y}}{\partial b_c}\,\middle|\,\frac{\partial\hat{y}}{\partial b}\,\middle|\,\frac{\partial\hat{y}}{\partial x_o}\right]$$

and

$$\frac{\partial \hat{x}_i}{\partial p} = \left[\begin{array}{c|c|c} \frac{\partial \hat{x}}{\partial \phi} & \frac{\partial \hat{x}}{\partial b_c} & \frac{\partial \hat{x}}{\partial x_o} \end{array}\right]$$

serves to indicate the corresponding component structure of these matrices. The values for $\partial \hat{x}_i/\partial p$ are generated by numerical integration of

$$\frac{d}{dt}\left(\frac{\partial \hat{x}_i}{\partial p}\right) = F(p)\frac{\partial \hat{x}_i}{\partial p} + \frac{\partial F(p)}{\partial p}\,\hat{x}_i + \frac{\partial G(p)}{\partial p}\,\hat{u}_i - G(p)\frac{\partial \hat{b}_c}{\partial b_c} \qquad \left(\begin{array}{l} \hat{x}_o = (\hat{x})_{t=0} \\ \dfrac{\partial \hat{x}_o}{\partial p} = \left[\begin{array}{c|c|c} 0 & 0 & \frac{\partial \hat{x}}{\partial x_o} \end{array}\right]_{t=0} \end{array}\right) \tag{8}$$

which is obtained by differentiation of equations (4) and (5). The elements of $\partial \hat{y}_i/\partial p$ and $\partial \hat{x}_i/\partial p$ form according to the rule for Jacobians, whereas those for the matrices resulting from the tensor products $\frac{\partial H(p)}{\partial p}\,\hat{x}_i$, $\frac{\partial D(p)}{\partial p}\,\hat{u}_i$, $\frac{\partial F(p)}{\partial p}\,\hat{x}_i$, and $\frac{\partial G(p)}{\partial p}\,\hat{u}_i$ are defined by

$$a_{ik} = \frac{\partial C}{\partial p}\,X = \sum_{j=1}^{M} \frac{\partial c_{ij}}{\partial p_k}\,x_j \tag{9}$$

The algorithm is further configured to provide options for deleting measurements from $y_{m,i}$ and for holding any combination of elements of $\hat{p}$ constant during the iterative solution process. To delete, say, the kth measurement from $y_{m,i}$, the kth row of $\partial \hat{y}_i/\partial p$ and kth element of $(y_{m,i} - \hat{y}_i)$ are set to zero. Holding the rth element of $\hat{p}$ constant is accomplished in a similar manner by setting the rth row of $\partial \hat{y}_i/\partial p$ to zero, but with the additional requirement that the rth element of the rth row of the resulting information matrix

$$\sum_{i=1}^{N} \left[\left(\frac{\partial \hat{y}_i}{\partial p}\right)^T \hat{R}^{-1} \left(\frac{\partial \hat{y}_i}{\partial p}\right)\right]$$ then be reset to have the value of unity instead of zero.

Aerodynamic Derivative Model

The linear perturbation model of the CH-47 dynamics employed in reference 2 is characterized by equation (4), which expresses the aircraft response relative to an equilibrium or nominal trim flight condition in terms of the control input and state vectors. Equations (10) and (11) define the extension of equations (3) and (4) to include modeling of the helicopter stability augmentation system (SAS) and are given in closed loop form by

$$y = \left[\begin{array}{c|c} H & GZ \end{array}\right] \left[\begin{array}{c} x \\ \hline v \end{array}\right] + [D]u + b \tag{10}$$

and

$$\frac{d}{dt}\left[\begin{array}{c} x \\ \hline v \end{array}\right] = \left[\begin{array}{c|c} F & GC \\ \hline KB & A \end{array}\right] \left[\begin{array}{c} x \\ \hline v \end{array}\right] + [G]u \qquad \begin{pmatrix} x_o = (x)_{t=0} \\ v_o = (v)_{t=0} \end{pmatrix} \tag{11}$$

in which the rigid body and SAS portions of the model are indicated by partitioning. The corresponding segments of the total state vector are denoted by x and v. The aerodynamic stability and control derivatives constitute the principal elements of the matrices H, D, F, and G, and those elements to be identified by means of equation (2) comprise the φ portion of the parameter vector p. The remaining matrix components GZ, GC, KB, and A pertain to the SAS model.

While originally included to permit verification of the model obtained by converting the SAS transfer functions given in reference 5 to state variable form (see ref. 3), the resulting SAS model also provides the useful option of performing derivative identification with either open or closed loop formulations. Equations (10) and (11) revert to open loop form by simply deleting the SAS terms; however, the effect of the SAS still must be taken into account since all flight tests were conducted on a closed loop basis with the SAS operating. This requirement is easily satisfied by adding the SAS output signals, which were measured as part of the CH-47 flight test data, to the control stick inputs. For verification against their measured values, analytical estimates of these commands are obtained from the SAS model by means of

$$\delta_{\theta,SAS} = v_1 \tag{12}$$

$$\delta_{\phi,SAS} = -K_p p \tag{13}$$

$$\delta_{\psi,SAS} = K_v v - K_r r + v_5 + v_7 \tag{14}$$

where the functions of the gains and state variables appearing in these formulas are subsequently indicated in the appropriate ones of equations (15) to (18). The numerical values used for all gains and other SAS model constants are listed in table I.

Although the derivatives tabulated in reference 2 are for the usual six degree-of-freedom formulation, the following expressions for the corresponding uncoupled longitudinal and lateral three degree-of-freedom representations were used in generating the MLE derivative values presented in this report. This simplification was made on the basis of the conclusion that both simulation studies (see ref. 3) and the actual flight data indicated the SAS uncouples these modes very well.

Longitudinal mode.- For the longitudinal motions of the helicopter, the respective three degree-of-freedom forms of equations (10) and (11) are

$$\begin{bmatrix} \theta \\ q \\ gn_x \\ gn_z \end{bmatrix} = \left[\begin{array}{cccc:ccc} 1 & 0 & 0 & 0 & 0 & 0 & 0 \\ 0 & 1 & 0 & 0 & 0 & 0 & 0 \\ 0 & X_q & X_w & X_u & X_{\delta_{long}} & 0 & 0 \\ 0 & Z_q & Z_w & Z_u & Z_{\delta_{long}} & 0 & 0 \end{array}\right] \left[\begin{array}{c} \theta \\ q \\ w \\ u \\ \hdashline v_1 \\ v_2 \\ v_3 \end{array}\right] + \begin{bmatrix} 0 & 0 \\ 0 & 0 \\ X_{\delta_{long}} & X_{\delta_{coll}} \\ Z_{\delta_{long}} & Z_{\delta_{coll}} \end{bmatrix} \begin{bmatrix} \delta_{long} \\ \delta_{coll} \end{bmatrix} + \begin{bmatrix} b_\theta \\ b_q \\ b_{n,x} \\ b_{n,z} \end{bmatrix} \tag{15}$$

and

$$\frac{d}{dt}\left[\begin{array}{c} \theta \\ q \\ w \\ u \\ \hdashline v_1 \\ v_2 \\ v_3 \end{array}\right] = \left[\begin{array}{cccc:ccc} 0 & 1 & 0 & 0 & 0 & 0 & 0 \\ 0 & M_q & M_w & M_u & M_{\delta_{long}} & 0 & 0 \\ -g \sin\Theta_o & Z_q + U_o & Z_w & Z_u & Z_{\delta_{long}} & 0 & 0 \\ -g \cos\Theta_o & X_q - W_o & X_w & X_u & X_{\delta_{long}} & 0 & 0 \\ \hdashline 0 & K_q b_1 & 0 & 0 & 0 & 1 & 0 \\ 0 & K_q b_2 & 0 & 0 & 0 & 0 & 1 \\ 0 & K_q b_3 & 0 & 0 & -a_o & -a_1 & -a_2 \end{array}\right] \left[\begin{array}{c} \theta \\ q \\ w \\ u \\ \hdashline v_1 \\ v_2 \\ v_3 \end{array}\right] + \begin{bmatrix} 0 & 0 \\ M_{\delta_{long}} & M_{\delta_{coll}} \\ Z_{\delta_{long}} & Z_{\delta_{coll}} \\ X_{\delta_{long}} & X_{\delta_{coll}} \end{bmatrix} \begin{bmatrix} \delta_{long} \\ \delta_{coll} \end{bmatrix} \tag{16}$$

for which the individual elements of the parameter vector p components are defined by

$$\varphi = \left[M_q M_w M_u Z_q Z_w Z_u X_q X_w X_u \; M\delta_{long} \; M\delta_{coll} \; Z\delta_{long} \; Z\delta_{coll} \; X\delta_{long} \; X\delta_{coll}\right]^T$$

$$b_c = \left[b\delta_{long} b\delta_{coll}\right]^T$$

$$b = \left[b_\theta b_q b_{n,x} b_{n,z}\right]^T$$

$$x_o = \left[\theta q w u\right]^T_{t=0}$$

Lateral-directional mode.- The corresponding three degree-of-freedom equations for the lateral helicopter motions are

$$\begin{bmatrix} p \\ r \\ \phi \\ gn_y \end{bmatrix} = \left[\begin{array}{cccc|cc} 0 & 1 & 0 & 0 & 0 & 0 \\ 0 & 0 & 1 & 0 & 0 & 0 \\ 0 & 0 & 0 & 1 & 0 & 0 \\ Y'_v & Y'_p & Y'_r & 0 & Y\delta_{rud} & Y\delta_{rud} \end{array}\right] \left[\begin{array}{c} v \\ p \\ r \\ \phi \\ \hline v_5 \\ v_7 \end{array}\right] + \begin{bmatrix} 0 & 0 \\ 0 & 0 \\ 0 & 0 \\ {}^{v}\delta_{lat} & Y\delta_{rud} \end{bmatrix} \begin{bmatrix} \delta_{lat} \\ \delta_{rud} \end{bmatrix} + \begin{bmatrix} b_p \\ b_r \\ b_\phi \\ b_{n,y} \end{bmatrix} \tag{17}$$

and

$$\frac{d}{dt}\begin{bmatrix} v \\ p \\ r \\ \phi \\ \hline v_5 \\ v_7 \end{bmatrix} = \left[\begin{array}{cccc|cc} Y'_v & Y'_p + W_o & Y'_r - U_o & g\cos\Theta_o & Y\delta_{rud} & Y\delta_{rud} \\ L^{*\prime}_v & L^{*\prime}_p & L^{*\prime}_r & 0 & L^{*}\delta_{rud} & L^{*}\delta_{rud} \\ N^{*\prime}_v & N^{*\prime}_p & N^{*\prime}_r & 0 & N^{*}\delta_{rud} & N^{*}\delta_{rud} \\ 0 & 1 & \tan\Theta_o & 0 & 0 & 0 \\ \hline 0 & 0 & K_r b_5 & 0 & -a_4 & 0 \\ 0 & K_{r,p} b_7 & 0 & 0 & 0 & -a_6 \end{array}\right] \left[\begin{array}{c} v \\ p \\ r \\ \phi \\ \hline v_5 \\ v_7 \end{array}\right] + \begin{bmatrix} Y\delta_{lat} & Y\delta_{rud} \\ L^{*}\delta_{lat} & L^{*}\delta_{rud} \\ N^{*}\delta_{lat} & N^{*}\delta_{rud} \\ 0 & 0 \end{bmatrix} \begin{bmatrix} \delta_{lat} \\ \delta_{rud} \end{bmatrix} \tag{18}$$

where the individual elements of the p vector components are given by

$$\varphi = \left[Y_v Y_p Y_r L^{*}_v L^{*}_p L^{*}_r N^{*}_v N^{*}_p N^{*}_r Y\delta_{lat} Y\delta_{rud} L^{*}\delta_{lat} L^{*}\delta_{rud} N^{*}\delta_{lat} N^{*}\delta_{rud}\right]^T$$

$$b_c = \left[b\delta_{lat} b\delta_{rud}\right]^T$$

$$b = \left[b_p b_r b_\phi b_{n,y}\right]^T$$

$$x_o = \left[vpr\phi\right]^T_{t=0}$$

and

$$Y_v' = Y_v + K_v Y_{\delta_{rud}}; \quad Y_p' = Y_p - K_p Y_{\delta_{lat}}; \quad Y_r' = Y_r - K_r Y_{\delta_{rud}}$$

$$L_v^{*\prime} = L_v^* + K_v L_{\delta_{rud}}^*; \quad L_p^{*\prime} = L_p^* - K_p L_{\delta_{lat}}^*; \quad L_r^{*\prime} = L_r^* - K_r L_{\delta_{rud}}^*$$

$$N_v^{*\prime} = N_v^* + K_v N_{\delta_{rud}}^*; \quad N_p^{*\prime} = N_p^* - K_p N_{\delta_{lat}}^*; \quad N_r^{*\prime} = N_r^* - K_r N_{\delta_{rud}}^*$$

which contain feedback terms corresponding to the respective gain elements in equations (13) and (14) for the roll SAS and yaw SAS commands. The roll and yaw derivatives are further modified according to

$$\begin{bmatrix} L_i^* \\ N_i^* \end{bmatrix} = \begin{bmatrix} \dfrac{1}{1 - \dfrac{I_{XZ}^2}{I_X I_Z}} \end{bmatrix} \begin{bmatrix} 1 & \dfrac{I_{XZ}}{I_X} \\ \dfrac{I_{XZ}}{I_Z} & 1 \end{bmatrix} \begin{bmatrix} L_i \\ N_i \end{bmatrix} \qquad (i = v,p,r,\delta_{lat},\delta_{rud}) \qquad (19)$$

which account for cross products of inertia ratios that couple the p and r equations. (See ref. 8.) Conversion of the identified derivatives to the format of reference 2 is given by the inverse relationships

$$\begin{bmatrix} L_i \\ N_i \end{bmatrix} = \begin{bmatrix} 1 & -\dfrac{I_{XZ}}{I_X} \\ -\dfrac{I_{XZ}}{I_Z} & 1 \end{bmatrix} \begin{bmatrix} L_i^* \\ N_i^* \end{bmatrix} \qquad (i = v,p,r,\delta_{lat},\delta_{rud}) \qquad (20)$$

and the values given in reference 2 for the CH-47 moments of inertia are

$$I_X = 50\ 386.3 \text{ kg m}^2$$

$$I_Z = 257\ 685 \text{ kg m}^2$$

$$I_{XZ} = 19\ 838.3 \text{ kg m}^2$$

Lastly, the trim values of U_o, W_o, and Θ_o appearing in equations (16) and (18) are listed in tables II to IV for each of the flight test runs.

PROCEDURE

The CH-47 flight tests were conducted for the conditions given in table V, which are representative of the landing approach trajectories of interest for the VALT program. The 15 principal test points listed involve a total of 44 individual runs and encompass most of the test plan presented in reference 3. As conventional pitot-static airspeed indicators are too inaccurate below about 50 knots, the time histories of the helicopter velocity for each run were obtained instead by means of precision radar tracking. (See ref. 4.) The corresponding wind magnitudes for correcting the velocity data to local freestream values were determined in the same manner by tracking weather balloons between successive runs and are also listed in table V.

Input Maneuvers

The test program set forth in table V includes runs for both manual and computer-generated input maneuvers. Due to the complexity of the piloting task, the former were limited to single control stick commands while the latter were implemented with both single and double ones as indicated. The manual inputs are of the usual doublet type, whereas those generated by means of the onboard computer consist of a long and a short period sinusoid described by

$$u(t) = \kappa(A_1 \sin \omega_1 t + A_2 \sin \omega_2 t) \tag{21}$$

and are depicted by the sketch accompanying table VI which lists the amplitude and frequency coefficients for each of the four basic helicopter control stick commands δ_{long}, δ_{coll}, δ_{lat}, and δ_{rud}. The frequencies of these sinusoids, for both the longitudinal and lateral dynamical modes, were chosen to correspond to the principal long and short period characteristic roots of equations (16) and (18). Each of the single input maneuvers for the runs at hover and at 20 knots were generated by evaluating equation (21) for only one of the four basic control stick commands, while the double input ones for the 40 and

60 knot runs employ a second such sinusoidal stick command commencing 6 sec later than the first one. The values entered in table VI for the starting times $t_{o,1}$ and $t_{o,2}$ permit combining δ_{coll} with δ_{long} and δ_{rud} with δ_{lat} as required for the runs listed in part (b) of table V. To avoid nonlinear responses, $A_2 \sin \omega_2 t$ of δ_{long} for the double input maneuvers is delayed 6 sec so that the two sinusoids occur separately instead of simultaneously.

In addition to the scale factor κ, which was included with the computer implementation of equation (21) to permit varying the amplitudes of the $u(t)$ so as to restrict the $y_{m,i}$ to linear values, a pilot stabilization model of the form

$$\delta_{long_{pilot}} = \kappa(0.2117u - 0.7867w) \tag{22}$$

was also programed. The use of $\delta_{long_{pilot}}$ was recommended to counter pitch response to δ_{lat} inputs, predicted by simulation results described in reference 3, that can cause large nonlinear changes in u of 9 m/sec or more at airspeeds of 40 knots and higher. According to reference 3, this response will occur because the long period pitch divergence mode becomes appreciably unstable at airspeeds of about 40 knots.

Data Processing

After completion of the basic data reduction, the flight data records were edited and then filtered to remove high frequency noise prior to arranging them in perturbation form for use in performing the derivative identification and model verification tasks. The filtering was accomplished by means of the digital filter of reference 9

$$d_i' = \bar{h}_o d_i + \sum_{i=1}^{N} \bar{h}_n (d_{i-n} + d_{i+n}) \qquad \begin{pmatrix} i > n \\ i = 1 \text{ to } S \end{pmatrix} \tag{23}$$

in which

$$d_{i-n} = d_{i+n} \qquad \begin{pmatrix} i \leq n \\ i = 1 \text{ to } S \end{pmatrix}$$

$$d_{i+n} = d_{i-n} \qquad \begin{pmatrix} i > (S - n) \\ i = 1 \text{ to } S \end{pmatrix}$$

and d_i' and d_i denote the filtered and unfiltered values of the ith sample of a measured quantity in a data record containing a total of S samples. Equation (23) is an alternate formula for the filter that is convenient for handling the beginning and ending portions of the data record where values of d_i that do not lie within $[1,S]$ are called for in the filtering process.

The weights h_k apply to $2N + 1$ of the S samples for each value of i and are normalized according to

$$\bar{h}_k = \frac{h_k}{h_c + 2\sum_{n=1}^{N} h_n} \tag{24}$$

in which each weight is divided by the sum of all $2N + 1$ values. The number of weights to be used, which depends on the cut-off and termination frequencies f_c and f_t and the sampling interval Δt, was determined by

$$N = \frac{2}{(f_t - f_c)\,\Delta t} \tag{25}$$

as recommended in reference 9.

The set of weighting functions h_n are generated by means of the formula

$$h_n = \frac{1}{2\pi n\,\Delta t}\left[\frac{\sin \omega_t\, n\,\Delta t + \sin \omega_c\, n\,\Delta t}{1 - 4(f_t - f_c)^2 (n\,\Delta t)^2}\right] \qquad (n = 1 \text{ to } N) \tag{26}$$

where $\omega = 2\pi f$. As equation (26) is indeterminate for $n = 0$, and for $n\,\Delta t = \frac{1}{2(f_t - f_c)}$ as well, the expression

$$h_n = \left[\frac{f_t \cos \omega_t\, n\,\Delta t + f_c \cos \omega_c\, n\,\Delta t}{1 - 12(f_t - f_c)^2 (n\,\Delta t)^2}\right] \qquad (n = 0 \text{ to } N) \tag{27}$$

obtained by means of L'Hôpital's rule is then used. Evaluation of equation (27) for $n = 0$ yields $h_o = f_t + f_c$ for the value of the central weight.

A typical example of the filter effectiveness in removing high frequency noise is illustrated by the solid curve plotted in figure 1, which represents the filtered roll rate time history from run 10. (See table IV.) The sampling rate and the cut-off and termination frequencies used to produce d_i' for this plot, and for all of the flight data, were $\Delta t = 1/40$ sec, $f_c = 1$ Hz, and $f_t = 2$ Hz. These choices resulted in the use of 151 weights since the corresponding value of N, as determined from equation (25), is 80.

After applying the wind corrections from table V and resolving the resulting freestream velocity components along the aircraft body axes, the remaining processing step was to represent the data as perturbations relative to equilibrium or trim flight conditions. This reduction only amounts to forming the differences between the total output response measurements $Y_{m,i}$ and their respective trim values $Y_{m,o}$ as indicated in figure 2.

For the ideal situation where the choice of $Y_{m,o}$ is free from error, the desired output response perturbation data is simply $y_{m,i} = Y_{m,i} - Y_{m,o}$ which also subtracts out any measurement bias. However, if problems such as unsteady trim conditions cause the selection of the trim point value to be in error as denoted by $Y'_{m,o}$ in figure 2, then $Y'_{m,o} = Y_{m,o} - b$ and the resulting perturbation data become

$$\begin{aligned} y'_{m,i} &= Y_{m,i} - Y'_{m,o} \\ &= Y_{m,i} - Y_{m,o} + b \\ &= y_{m,i} + b \end{aligned}$$

so that the effect of the trim point selection error is to introduce a bias b into all i values of $y'_{m,i}$. Note that the small Δt_o time offset between $Y'_{m,o}$ and $Y_{m,o}$ has no effect other than to shift the time at which $y'_{m,i}$ starts and does not contribute any lead or lag. The bias estimate term in equation (3) was included mainly as a means to compensate for the trim error biases just described. Equation (5) was similarly structured since essentially the same situation occurs with the control input measurements.

MLE Derivative Identification

The computation of $\hat{\varphi}$ by means of the MLE algorithm given by equation (2) was not entirely successful since some of the test runs in table V were compromised by dropouts in the radar measurements and failure to achieve good trim conditions prior to initiating the test maneuvers.

The dropouts often caused uncertainty in determining the trim values of U_o and W_o required in evaluating equations (16) and (18) and precluded obtaining any values for them at all for some of the runs. This problem further prevented including the velocity perturbation measurements $u_i = U_i - U_o$, $v_i = V_i - V_o$, and $w_i = W_i - W_o$ as elements of the $y_{m,i}$ vector in the appropriate one of equations (15) and (17). Inspection of equations (15) to (18),

however, shows the derivative information contained in these measurements essentially duplicates that of the linear accelerations n_x, n_y, and n_z so that omission of u, v, and w does not impair or prevent derivative identification. Thus, no further attempt was made to use u, v, or w as response measurements in generating any of the MLE results.

The consequences of inadequate trim conditions gave rise to a more serious problem which in effect is equivalent to modeling error. Unsteady trims can introduce appreciable linear and angular acceleration contributions to the aircraft response motions that are assumed to be negligible in postulating the linear perturbation model. (See ref. 8.) Since the dynamical models defined by equations (16) and (18) do not correctly describe the aircraft response under such conditions, the MLE algorithm then cannot yield accurate derivative estimates. The trim conditions assumed in stating these equations are that $V_o = P_o = Q_o = R_o = 0$ and that U_o and W_o have constant values. Typical values for these quantities are illustrated by the curves in figure 3 which are plotted for run 18 from test point 5. (See table V.)

Due to the changing values of the trim variables, the magnitudes of the corresponding acceleration contributions can vary sharply and can cause the convergence characteristics of $\hat{\varphi}$ to be very sensitive to the choice of the initial time t_o from which the test maneuver is presumed to start. A change in t_o of only 1/40 sec, for example, caused divergent solutions to converge and vice versa for some of the test runs. The MLE derivative identification computations with the present flight data usually yielded convergent solutions for $\hat{\varphi}$ when t_o could be chosen such that the trim values of the linear and angular accelerations were within about 0.3 m/sec^2 and 0.5 deg/sec^2, respectively. The slopes of the curves plotted in figure 3 show that these limits cannot be satisfied for any usable choice of t_o, which apparently is the primary reason a convergent solution was not obtained for run 18. The best $\hat{\varphi}$ attempt occurred for $t_o = 2$ sec as marked on the plots in figure 3 but diverged on the 20th iteration.

Unsteady trim conditions also appeared to be causally related to the slow convergence observed for several of the other test runs, which is characteristic of the solution behavior in the presence of modeling error. Convergence of equation (2) typically required 10 to 20 iterations, compared with 5 to 8 iterations for solutions based on the use of simulated $y_{m,i}$ data which contained no modeling error. Coincidentally, the values of $\hat{\varphi}$ were often distorted from realistic levels, and those for $\hat{b}$, $\hat{b}_c$, and $\hat{x}_o$ were usually much larger than the maximum error that could possibly be introduced in forming $y_{m,i}$ and $u_{m,i}$. The fact that including $\hat{b}$ and $\hat{b}_c$ in $\hat{p}$ caused the solutions for some runs to converge - albeit to physically incorrect values which were nonconvergent when only the $\hat{\varphi}$ were estimated - further indicates modeling error. Additionally, the values for $\hat{\varphi}$, $\hat{b}$, $\hat{b}_c$, and $\hat{x}_o$ were all correctly and accurately determined when identified from simulated data containing only measurement error.

These results are consistent with the well known fact that the minimization process embodied in equation (2) will vary all of the elements of $\hat{p}$, in accordance with the analytical structure of the $\hat{x}_i$ and $\hat{y}_i$ models, so as to minimize $(y_{m,i} - \hat{y}_i)$ in the least squares sense. (See ref. 10.) When modeling

error is present, the estimated parameters therefore become more and more distorted as the rank of $\hat{p}$ increases. The MLE algorithm then will in essence "misuse" $\hat{b}$, $\hat{b}_c$, and $\hat{x}_o$ to fit modeling error; this explains why generally better results were obtained when only the elements of $\hat{\varphi}$ were identified. Thus, the acceleration contributions arising from inadequate trim conditions appear to be a more likely source of modeling error than model structure considerations associated with the rank of $\hat{p}$ or with the models for $\hat{x}_i$ and $\hat{y}_i$ assumed in equations (16) to (18). Evaluating the effect of such errors on the computed response time histories, as well as on the accuracy of $\hat{\varphi}$, accordingly represents an important part of the overall model verification task.

RESULTS AND DISCUSSION

The principal steps in verifying the linear perturbation model of reference 2 were to compare the respective estimated and measured output response time histories $\hat{y}_i$ and $y_{m,i}$ and to compare the corresponding analytical derivatives with the EKF and MLE values identified from the flight data. These comparisons accordingly involve three sets of $\hat{y}_i$ which were generated using the analytical derivatives of reference 2, the EKF values of reference 4, and the MLE estimates of $\hat{\varphi}$ from equation (2). As stated in reference 4, the EKF derivatives were obtained using a six degree-of-freedom model subsequent to preprocessing the flight data with a Kalman filter based on kinematical relationships. The effect of the SAS is taken into account in the EKF algorithm by adding the measured SAS signals directly to the control inputs in the equivalent open loop fashion described in connection with equations (10) and (11). Since the analysis being presented assumes decoupled three degree-of-freedom dynamical modes, the three sets of $\hat{y}_i$ for each of the longitudinal and lateral-directional runs listed in table V were obtained separately by evaluating equation (15) or (17) as appropriate. The corresponding time histories of $\hat{x}_i$ required in these computations were generated by numerically integrating equations (16) and (18) using the fourth-order Runge-Kutta method with a fixed step size of 0.10 sec.

In order to avoid an unwieldy volume of plotted and tabulated data, which contributes little additional information, only results of runs from test points 2, 3, 5, 7, 10, 13, and 15 of table V are presented. An exception is run 33 from test point 11, which is included in connection with model structure verification. The results from the single input runs in test points 2, 3, and 5 that involve δ_{coll} and δ_{rud} were also omitted as being unnecessary for the purposes herein. All of the manual input runs were eliminated from further consideration in the early stages of the derivative identification computations because these data did not yield convergent solutions for $\hat{\varphi}$. Most of these runs resulted in $y_{m,i}$ values that exceeded acceptable small perturbation bounds and generally exhibited poor excitation of both the short and long period response modes.

In generating the MLE solutions, the reference 2 derivatives were always used for $\hat{\varphi}_o$ in equation (2) since they represented the best available starting values for initiating the iteration process. Because the $y_{m,i}$ responses to single input maneuvers contain no information about the control derivatives

corresponding to the omitted input other than through feedback (see eqs. (15) to (18)), these derivatives were not estimated and were held constant at their reference 2 initial values for all such runs. This fact is indicated by the parenthetically marked entries in tables II and IV.

Longitudinal Derivatives and Response Time Histories

The time histories $\hat{y}_i$ and $y_{m,i}$ for the seven longitudinal runs 5, 9, 17, 25, 31, 39, and 43 from test points 2, 3, 5, 7, 10, 13, and 15 of table V are plotted in figures 4(a) to 4(g), and the corresponding derivative values and trim conditions are listed in table II. No MLE results are presented for runs 9 and 25 because convergence of $\hat{\varphi}$ was apparently prevented by the data problems discussed previously. Comparisons with the EKF method are made for only five of the seven runs since derivative values for the other two are not given in reference 4. To investigate the validity of the model structure assumed in equation (16) for the longitudinal mode, the results for run 33 of test point 11 from two different flights are compared in figure 5 and table III.

By referring to figure 4, reasonable agreement between the $\hat{y}_i$ generated from the analytical derivative values of reference 2 and the $y_{m,i}$ flight data is seen to exist for all seven runs, with some exceptions. These concern the presence of unmodeled response motion and discrepancies in the $\hat{y}_i$ response characteristics associated with the values of the modeled stability and control derivatives. Mention should be made of the fact that pilot model inputs as given by equation (22) were inadevertently added to δ_{long} for runs 33 (flight 035), 39, and 43. Other than to slightly distort the sinusoidal structure of δ_{long}, the addition of $\delta_{long_{pilot}}$ to these runs did not appear to create problems or affect derivative identification.

Unmodeled response.- The time histories plotted in figure 4 show an oscillatory contribution to the response motion that occurs at nearly the damped natural frequency of the longitudinal short period mode and is not predicted by equation (16) for either of the three sets of derivatives listed in table II. This unmodeled response appears mainly in the n_x plots but is also evident in those for q, n_z, and $\delta_{\theta,SAS}$ for some runs. These effects, which are most prominent in runs 5, 17, and 25, are almost absent from runs 31, 39, 43, and both runs 33 in figure 5. Although hysteresis and nonlinearity in the CH-47 control system (or perhaps rotor dynamics) represent possible sources, the cause of the unmodeled response motion was not determined.

Variation in longitudinal response characteristics.- The second area of disagreement exhibited by the $\hat{y}_i$ plots in figure 4 pertains to differences between the characteristics of the measured and computed responses to mainly the short period component $A_1 \sin \omega_1 t$ of both δ_{long} and δ_{coll} inputs. (See eq. (21).) The results for all seven runs show the responses to $A_1 \sin \omega_1 t$ of each type input, as generated using the reference 2 derivatives, to occur at slightly higher frequencies and with smaller amplitudes than the measured data. Although there may be some contribution to these differences from unmodeled accelerations arising from unsteady trim conditions, incorrect stability and control derivatives also can affect the response characteristics

of the computed time histories. The fact that the plots in figure 4 show differences between the $\hat{y}_i$ from the reference 2 and MLE derivatives strongly suggests that error in these parameters probably accounts for most of the disagreement with the $y_{m,i}$ data.

In order to determine which derivatives dominate these variations in response characteristics, several families of $\hat{y}_i$ sensitivity curves were generated in which each of the 15 derivatives modeled in equation (16) were set to zero one at a time. These plots, which were computed from the reference 2 derivatives for airspeeds of 0, 20, 40, and 60 knots, indicate that the frequency and damping characteristics of the $\hat{y}_i$ are most sensitive to changes in M_q. Reference to table II suggests that the reference 2 values for M_q are too large, which thus appears to be the main reason the frequency and damping of the corresponding short period responses are accordingly too large. The $\hat{y}_i$ generated from the MLE derivatives tend to agree more closely with the $y_{m,i}$, but the values for M_q may be somewhat too small, particularly at the higher airspeeds. Except for runs 17 and 25, the EKF results also indicate the reference 2 values for M_q are too large and agree better with the MLE estimates.

In addition to showing the short period damping to be dominated mainly by M_q, the sensitivity plots further indicate the amplitudes of the $\hat{y}_i$ responses to δ_{long} and δ_{coll} inputs to be approximately proportional to the magnitudes of the corresponding control derivatives, as expected. The pitch rate time histories plotted in figure 4 thus indicate that the reference 2 and MLE values for $M_{\delta_{long}}$ listed in table II are of about the correct magnitudes, while those for the EKF model appear to be three to four times too small. Similarly, the plots of n_x suggest that the MLE values for $X_{\delta_{long}}$ are reasonably correct and that those for the other two models are an order of magnitude too small. The plots of n_z exhibit about the same behavior for the runs at hover and 20 knots, except that the sign of $Z_{\delta_{long}}$ also appears to be incorrect for the reference 2 and EKF models. The three sets of $Z_{\delta_{long}}$ values are in better agreement for the runs at 40 and 60 knots; however, the sensitivity plots indicate that damping of the n_z responses is also strongly affected by Z_w. These results show the MLE estimates of Z_w for runs 31 and 39 to be of incorrect sign and imply that the reference 2 values are perhaps a factor of 2 too large. The δ_{coll} control derivatives for the three derivative models agree more closely than those for δ_{long} and do not give rise to any large differences between the amplitudes of $\hat{y}_i$ and $y_{m,i}$.

Pitch SAS model.- The plots for $\delta_{\theta,SAS}$ in figure 4 (and also in fig. 5) generally exhibit the same response characteristics as would be expected for q since the SAS states v_1, v_2, and v_3 are dominated by the pitch rate response. (See eqs. (12) and (16).) These curves indicate about the same level of agreement between the measured pitch SAS time histories and those predicted by each of the three sets of derivatives. Thus, the $\delta_{\theta,SAS}$ results tend to verify the pitch SAS modeling employed in equations (15) and (16).

Model structure.- The comparison of results from two different trials of run 33 from test point 11, presented in figure 5 and table III, provides data for investigating the validity of the model structure assumed in equation (16) and represents an important aspect of the overall model verification task as previously discussed. In figure 5(a), and vice versa in figure 5(b), the $\hat{y}_i$ generated by the $\hat{\varphi}$ identified using the plotted $y_{m,i}$ are compared with both the $\hat{y}_i$ computed with the $\hat{\varphi}$ from the other run and the $\hat{y}_i$ from the reference 2 derivatives. Both sets of results indicate relatively minor degradation of the curve fit when $\hat{\varphi}$ from a different trial of the same run is used to generate $\hat{y}_i$. The agreement between $y_{m,i}$ and the MLE estimates of $\hat{y}_i$ from both runs indicated in figure 5 and table III does not, therefore, appear to be just the result of satisfying the MLE minimization criteria but represents limited verification of equation (16). As the trim conditions for both runs were generally better than those for most of the other higher airspeed runs, the degradation in accuracy of the $\hat{\varphi}$ due to nonzero accelerations in the $y_{m,i}$ is probably not very great.

Lateral-Directional Derivatives and Response Time Histories

The time-history comparisons for the seven lateral runs 6, 10, 18, 26, 32, 40, and 44 from test points 2, 3, 5, 7, 10, 13, and 15 are plotted in figures 6(a) to 6(g), and the corresponding derivatives and trim conditions are listed in table IV. As with runs 9 and 25, data problems apparently prevented convergence of $\hat{\varphi}$ so that no MLE results for run 18 are presented. The EKF results for run 18 are also omitted since they appeared to be similarly affected by the same data problems. Comparisons with the EKF method accordingly were made for just four of the seven runs because the necessary derivative values for runs 10 and 44 are not given in reference 4. Unfortunately, none of the MLE solutions for the lateral runs provided suitable duplicate data for model structure verification of equation (18), as was done with equation (16).

The results presented in figure 6 generally indicate about the same level of agreement between $\hat{y}_i$ from the reference 2 derivatives and the $y_{m,i}$ flight data as for the longitudinal runs and exhibit similar discrepancies as well. Although no unintentional pilot model implementation occurred with the lateral runs, the fact should be mentioned that the δ_{lat} inputs for runs 26 and 32 contain an unprogramed signal of undetermined origin which is not modeled by equation (21). This signal resembles the pilot model input given by equation (22); however, the amplitude variations in u and w over the relevant portions of their time histories are too small in both runs to generate a $\delta_{long_{pilot}}$ comparable to the input signal in question. While the source of this signal was therefore not the pilot stabilization model, its presence appeared to have no noticeable effect on the results.

Unmodeled response.- The time history plots in figure 6 show an unmodeled oscillatory contribution to $\hat{y}_i$ similar to that noted in figure 4; however, the frequency is generally higher relative to that of the lateral short period mode and the amplitude is smaller. As with the longitudinal runs, the unmodeled response is most prominent in the linear acceleration plots. This behavior, which is not predicted by equation (18) for either of the three sets of deriva-

tives listed in table IV, is evident in the n_y curves for all seven runs and in the $\delta_{\psi,SAS}$ plots for runs 6 and 10 also. The period of this oscillation appears to be about 1 sec or roughly half that observed for the ones in the longitudinal runs. As in the case of the longitudinal mode, the cause of the unmodeled response was not identified.

Variation in lateral-directional response characteristics.- The characteristics of the measured and computed responses to the $A_1 \sin \omega_1 t$ component of δ_{lat} and δ_{rud} inputs exhibit differences that are similar to those noted for the longitudinal runs. In the same manner as for equation (16), sensitivity time histories were generated for the 15 derivatives modeled in equation (18). These plots were also computed for airspeeds of 0, 20, 40, and 60 knots using the reference 2 derivatives. They indicate that variation in L_p has the most effect on the lateral-directional short period frequency and damping characteristics.

Examination of the $\hat{y}_i$ plots in figure 6 and the entries in table IV suggests that the reference 2 values for L_p are perhaps 20 percent too small for the hover and 20 knot runs, and roughly the same amount too large for the runs at 40 and 60 knots. By comparison, the MLE estimates of L_p yield $\hat{y}_i$ that agree more closely with the $y_{m,i}$ at the lower airspeeds, but the entries for the higher airspeeds appear slightly too small except for run 44. With the exception of run 40, all of the EKF values for L_p are of positive sign as noted in reference 4. The positive values for L_p result in insufficient damping of the lateral-directional short period mode and cause some of the $\hat{y}_i$ in figure 6 to exhibit divergence. (See fig. 6(a) for example.)

With regard to amplitude, the principal areas of disagreement between $\hat{y}_i$ and $y_{m,i}$ concern the curves for p and n_y plotted in figure 6. The derivative sensitivity plots indicate that the differences in the response amplitudes of p to δ_{lat} inputs are not due to the damping action of L_p alone. The plotted results thus imply that the values for $L_{\delta_{lat}}$ listed in table IV are too small by 30 percent or more for all three derivative models. The curves for n_y show 180° phase differences in the responses to both δ_{lat} and δ_{rud} inputs that indicate the reference 2 and EKF values for the lateral force control derivatives have incorrect signs. The entries in table IV and the n_y plots generated from the MLE derivatives suggest that $Y_{\delta_{lat}}$ should be negative for all seven runs with approximately the magnitudes of the reference 2 values. Similarly, $Y_{\delta_{rud}}$ should remain positive with magnitudes somewhat larger than the MLE estimates.

Roll SAS and yaw SAS models.- In a manner analogous to the $\delta_{\theta,SAS}$ plots in figures 4 and 5, the time histories of $\delta_{\phi,SAS}$ and $\delta_{\psi,SAS}$ presented in figure 6 exhibit about the same response characteristics as those for p and for the composite of r and n_y, as would be inferred from equations (13), (14), and (18). The measured and computed SAS signals again reflect the same level of agreement as that between the $y_{m,i}$ and the three sets of $\hat{y}_i$, except that the amplitudes of the roll SAS measurements are 10 to 20 percent larger than predicted by either of the three derivative models. The reason appears

to be that canceling one of the two roll SAS actuators to halve the roll SAS gain K_p (see table I), as recommended in reference 3 to minimize rotor-fuselage coupling predicted by simulation studies, did not yield exactly the desired 6.35 value. However, the results plotted in figure 6 do not otherwise indicate any deficiencies which would invalidate the SAS models incorporated in equations (17) and (18).

Closed Loop MLE Derivative Identification

As mentioned in the Introduction, one of the objectives of the overall model verification was to investigate the effect on derivative identification of conducting the flight tests on a closed loop basis with the SAS operating. The preliminary checkout of the MLE algorithm for the CH-47 application, using simulated $y_{m,i}$ data which include the effects of the SAS, indicated that good closed loop identification accuracy should be attainable with reasonably consistent flight data. The MLE results presented in figures 4 to 6 and tables II to IV strongly suggest that comparable accuracy also would have been achieved with the actual flight data if the trim conditions had been more adequately obtained. Although the modeling error introduced by inadequate trim conditions may retard or even prevent convergence of the MLE algorithm, the checkout computations further showed that no increase in the number of iterations of equation (2) should occur because of performing derivative identification with a closed loop dynamical system.

The notions that the SAS will suppress response modes and cause what is termed masking of the derivatives, so as to reduce or impair their identifiability, were not observed to be true of the $\hat{\varphi}$ computations with either simulated or actual flight data. To the contrary, the plots of $y_{m,i}$ in figures 4 to 6 show well defined responses with no evidence of any suppression of either the short or long period modes. By preventing divergent responses, the SAS thus appears to facilitate rather than impede good modal excitation. In addition to decoupling the longitudinal and lateral-directional modes very effectively, as discussed in conjunction with equations (15) to (18), the SAS also seems to enhance the identifiability of the control derivatives when the MLE algorithm is used.

Comparison of Manual and Computer-Generated Input Maneuvers

The primary purpose in comparing results from manual and computer-generated input maneuvers is to evaluate the suitability of each for generating flight data for derivative identification purposes. In this connection, the most important requirement for the response data is good excitation of the aircraft dynamic modes at the largest amplitudes that remain within practical small perturbation bounds. The $y_{m,i}$ curves for run 36 plotted in figure 7 and for run 40 in figure 6 illustrate typical response measurements generated by manual and computer-generated inputs at the same test conditions. Although the plots in figure 7 are not representative of typical pilot performance in any sense because no practice maneuvers were flown, they do however demonstrate inherent difficulties that can be encountered in manually implementing a doublet pulse input maneuver having the desired frequency and amplitude characteristics. In

this example, the amplitude of the δ_{lat} input is satisfactory but the frequency is almost three times less than the value for ω_i listed in table VI. Primarily because the pulse duration is thereby too long, the resulting amplitude of p (see fig. 7) is too large and is seen to be roughly double that produced by the corresponding computer-generated δ_{lat} input maneuver. The manual inputs also are not very repeatable, as both the pulse duration and amplitude are usually determined by the pilot's judgment with the result that accurate repetition of even the most simple doublet pulse is almost impossible to achieve. Furthermore, the complexity of the piloting task essentially prohibits using inputs that require superimposing multiple pulses of differing frequency and amplitude content.

Computer-generated inputs, by comparison, exhibit the potential for alleviating practically all of the difficulties just described. The results presented in figures 4 to 6 indicate that these inputs can solve the problem of response mode excitation very successfully. Most of the $y_{m,i}$ curves show well-defined sinusoids that have precisely the intended short and long period response frequencies. In this connection, using the variable scale factor κ (see eq. (22)) proved to be highly effective in constraining the response amplitudes of the $y_{m,i}$ in these runs within practical linearity limits.

The onboard computer, by providing the capability for programing any variety and number of input shapes or waveforms that can be represented mathematically, thereby offers the means for assuring proper modal excitation which effectively solves the most difficult part of the input design problem. The remaining task then concerns determining an optimum combination of the number of sinusoids or other input shapes, their frequencies and amplitudes, and the number of cycles each one is to be repeated during the course of the input maneuver. Since they can be precisely repeated as often as desired once programed, these inputs also can facilitate generating duplicate $y_{m,i}$ data for model structure verification. Thus, when the test aircraft is equipped with the necessary electronic control system, the use of computer-generated inputs appears to be superior to manual ones. Subsequent flight tests for other purposes showed that very good trim conditions can be achieved by means of the electronic control system. Hence, the problem with nonzero trim accelerations can be largely avoided by also automating the trimming of the aircraft prior to initiating a test maneuver.

CONCLUSIONS

The results from flight tests for verifying an existing analytical model of the aerodynamic derivatives for a CH-47 tandem-rotor transport helicopter indicate the following conclusions:

1. The analytical model is reasonably correct with respect to the stability derivatives, which exhibit only minor inaccuracies, but some of the longitudinal and lateral force control derivatives have incorrect signs and magnitude errors as large as a factor of 10.

2. Although nonzero trim accelerations in the flight data caused the derivatives identified from both extended Kalman filter (EKF) and maximum likelihood

estimator (MLE) algorithms to be in error also, the results from the latter show a strong tendency to correct the deficiencies in the analytical model that indicates the MLE algorithm would yield good accuracy if trim accelerations were absent.

3. Closed loop flight testing with the aircraft stability augmentation system (SAS) operating does not adversely affect derivative identification for tandem-rotor helicopters.

4. The use of computer-generated input maneuvers is superior to manual ones and is highly effective in generating transient response data having good modal excitation without exceeding practical small perturbation amplitude bounds.

5. Whenever the necessary electronic control system is available, the problem with nonzero trim accelerations should be largely avoidable by also automating the trimming of the aircraft prior to initiating a test maneuver.

Langley Research Center
National Aeronautics and Space Administration
Hampton, VA 23665
November 21, 1979

REFERENCES

1. Kelly, James R.; Niessen, Frank R.; Thibodeaux, Jerry J.; Yenni, Kenneth R.; and Garren, John F., Jr.: Flight Investigation of Manual and Automatic VTOL Decelerating Instrument Approaches and Landings. NASA TN D-7524, 1974.

2. Ostroff, Aaron J.; Downing, David R.; and Rood, William J.: A Technique Using a Nonlinear Helicopter Model for Determining Trims and Derivatives. NASA TN D-8159, 1976.

3. Hall, W. E., Jr.; and Vincent, J.: Flight Test Design for CH-47 Parameter Identification. NASA CR-158948, 1978.

4. Tomaine, R. L.; Bryant, W. H.; and Hodge, W. F.: VALT Parameter Identification Flight Test - VTOL Approach and Landing Technology. Paper presented at Fourth European Rotorcraft and Powered Lift Aircraft Forum (Stresa, Italy), Sept. 13-15, 1978.

5. Davis, J. M.: Stability and Control Analysis. No. 114-AD-603 (Contract DA23-204-AMC-04366 (Y)), Vertol Div., Boeing Co., Nov. 28, 1966.

6. Iliff, Kenneth W.; and Taylor, Lawrence W., Jr.: Determination of Stability Derivatives From Flight Data Using a Newton-Raphson Minimization Technique. NASA TN D-6579, 1972.

7. Hodge, Ward F.; and Bryant, Wayne H.: Monte Carlo Analysis of Inaccuracies in Estimated Aircraft Parameters Caused by Unmodeled Flight Instrumentation Errors. NASA TN D-7712, 1975.

8. McRuer, Duane; Ashkenas, Irving; and Graham, Dunstan: Aircraft Dynamics and Automatic Control. Princeton Univ. Press, 1973.

9. Graham, Ronald J.: Determination and Analysis of Numerical Smoothing Weights. NASA TR R-179, 1963.

10. Taylor, Lawrence W., Jr.: Application of a New Criterion for Modeling Systems. Methods for Aircraft State and Parameter Identification, AGARD-CP-172, Nov. 1974, pp. 4-1 - 4-9.

TABLE I.- CH-47 SAS MODEL CONSTANTS

Feedback gains:	
K_q, cm/rad/sec	43.94
[a] K_p, cm/rad/sec	6.35
K_r, cm/rad/sec	26.21
$K_{r,p}$, cm/rad/sec	16.43
K_v:	
$\bar{U}_o$ = 0 to 20 knots, cm/m/sec	0
$\bar{U}_o$ = 20 to 40 knots, cm/m/sec	0.1233
$\bar{U}_o$ = 40 to 60 knots, cm/m/sec	0.2717
$\bar{U}_o$ = 60 to 80 knots, cm/m/sec	0.2958
State variable coefficients:	
a_0	0.0364
a_1	0.8177
a_2	3.0401
[b] a_4	0.3125
a_6	0.2433
Feedback gain coefficients:	
b_1	-1.2890
b_2	3.2676
b_3	-8.8799
b_5	0.3125
b_7	0.2433

[a] Value one-half that given in reference 5. (See also ref. 3.)
[b] $a_4 = 2a_4$; $\bar{U}_o$ < 40 knots.

TABLE II.- LONGITUDINAL AERODYNAMIC DERIVATIVES AND TRIM CONDITIONS

Quantity	Derivative model (a)	Run 5	Run 9	Run 17	Run 25	Run 31	Run 39	Run 43
$\bar{U}_o$, knots		0	0	20	40	40	60	60
$\bar{W}_o$, m s^{-1}		0	2.54	2.54	0	2.54	0	2.54
Trim:								
U_o, knots		1.7	1.0	18.4	44.9	41.2	62.8	63.2
W_o, m s^{-1}		-0.00	2.15	3.67	-0.00	2.78	0.93	3.71
Θ_o, deg		6.36	7.42	3.90	3.20	5.31	2.49	1.91
Stability:								
M_q, s^{-1}	○	-1.2293	-1.2486	-1.3422	-1.5695	-1.6084	-1.6818	-1.7072
M_q, s^{-1}	□	-0.8882	-------	-0.6005	-------	-0.4776	-0.5159	-0.2911
M_q, s^{-1}	◇	-0.6680	-------	-0.1471	-1.6089	-0.4633	-0.6040	-------
M_w, s^{-1} m^{-1}	○	0.0077	0.0094	0.0402	0.0583	0.0680	0.0579	0.0623
M_w, s^{-1} m^{-1}	□	-0.0284	-------	0.2248	-------	-0.0591	0.0480	0.0097
M_w, s^{-1} m^{-1}	◇	-0.0496	-------	-0.0483	-0.0363	-0.0157	-0.0107	-------
M_u, s^{-1} m^{-1}	○	0.0304	0.0445	0.0317	-0.0034	-0.0076	-0.0138	-0.0170
M_u, s^{-1} m^{-1}	□	0.0321	-------	0.0126	-------	-0.0239	-0.0013	0.0100
M_u, s^{-1} m^{-1}	◇	0.0344	-------	0.0009	0.0014	-0.0008	-0.0157	-------
Z_w, s^{-1}	○	-0.2956	-0.2598	-0.3155	-0.4454	-0.4155	-0.5512	-0.5345
Z_w, s^{-1}	□	0.1203	-------	-0.4121	-------	0.4107	0.0758	-0.2266
Z_w, s^{-1}	◇	0.0454	-------	-0.5977	-0.0429	-0.1055	-0.1550	-------
X_w, s^{-1}	○	0.0326	0.0289	0.0322	0.0387	0.0385	0.0376	0.0390
X_w, s^{-1}	□	0.2425	-------	0.1947	-------	-0.0117	0.0755	-0.0340
X_w, s^{-1}	◇	0.0382	-------	0.0180	0.0315	0.0436	0.0201	-------
X_u, s^{-1}	○	-0.0211	-0.0186	0.0013	-0.0116	-0.0093	-0.0205	-0.0192
X_u, s^{-1}	□	-0.0690	-------	-0.0126	-------	-0.0383	-0.0304	0.0001
X_u, s^{-1}	◇	-0.0429	-------	-0.0323	-0.0358	-0.0154	-0.0483	-------
Control:								
$M\delta_{long}$, s^{-2} cm^{-1}	○	0.1296	0.1258	0.1289	0.1401	0.1395	0.1540	0.1549
$M\delta_{long}$, s^{-2} cm^{-1}	□	0.1116	-------	0.1577	-------	0.1080	0.1397	0.1278
$M\delta_{long}$, s^{-2} cm^{-1}	◇	0.0588	-------	0.0129	0.0206	0.0313	0.0473	-------
$M\delta_{coll}$, s^{-2} cm^{-1}	○	0.0075	0.0069	0.0013	0.0359	0.0392	0.0602	0.0662
$M\delta_{coll}$, s^{-2} cm^{-1}	□	[b](0.0075)	-------	[b](0.0013)	-------	0.0137	0.0187	0.0306
$M\delta_{coll}$, s^{-2} cm^{-1}	◇	-0.0055	-------	-0.0033	0.0115	0.0254	0.0117	-------
$Z\delta_{long}$, m s^{-2} cm^{-1}	○	0.0036	0.0038	0.0199	0.0444	0.0512	0.0561	0.0630
$Z\delta_{long}$, m s^{-2} cm^{-1}	□	-0.1608	-------	-0.1466	-------	0.1184	0.1106	0.0355
$Z\delta_{long}$, m s^{-2} cm^{-1}	◇	0.0037	-------	0.0142	0.0206	0.0604	0.0853	-------
$Z\delta_{coll}$, m s^{-2} cm^{-1}	○	-0.9674	-0.9661	-0.9784	-1.0282	-1.0013	-1.1232	-1.0990
$Z\delta_{coll}$, m s^{-2} cm^{-1}	□	[b](-0.9674)	-------	[b](-0.9784)	-------	-0.7883	-0.6667	-0.7668
$Z\delta_{coll}$, m s^{-2} cm^{-1}	◇	-0.7836	-------	-1.1295	-1.1296	-0.6787	-0.7812	-------
$X\delta_{long}$, m s^{-2} cm^{-1}	○	0.0137	0.0131	0.0126	0.0130	0.0125	0.0152	0.0150
$X\delta_{long}$, m s^{-2} cm^{-1}	□	0.1514	-------	0.1784	-------	0.1363	0.1744	0.1257
$X\delta_{long}$, m s^{-2} cm^{-1}	◇	0.0141	-------	0.0269	0.0143	0.0121	0.0137	-------
$X\delta_{coll}$, m s^{-2} cm^{-1}	○	0.1126	0.1125	0.0831	0.0655	0.0661	0.0512	0.0550
$X\delta_{coll}$, m s^{-2} cm^{-1}	□	[b](0.1126)	-------	[b](0.0831)	-------	0.0444	0.0568	0.0670
$X\delta_{coll}$, m s^{-2} cm^{-1}	◇	0.0980	-------	0.0743	0.0655	0.0642	0.0523	-------

[a]○ Reference 2 □ MLE ◇ EKF (ref. 4).
[b]Held constant at reference 2 values.

TABLE III.- LONGITUDINAL AERODYNAMIC DERIVATIVES AND TRIM CONDITIONS

FOR RUN 33 FROM TWO DIFFERENT FLIGHTS

Quantity	Reference 2 ○	Flight 031 □	Flight 035 ◇
Trim:			
U_o, knots	40	41.7	39.6
W_o, m s^{-1}	5.08	5.52	6.61
Θ_o, deg	4.68	3.55	3.66
Stability:			
M_q, s^{-1}	-1.6547	-1.1070	-0.5236
M_w, s^{-1} m^{-1}	0.0790	-0.1195	-0.1030
M_u, s^{-1} m^{-1}	-0.0149	0.1803	-0.0262
Z_w, s^{-1}	-0.3849	-0.3612	-0.4440
X_w, s^{-1}	0.0384	-0.1071	-0.1217
X_u, s^{-1}	-0.0069	0.2145	-0.0305
Control:			
$M_{\delta_{long}}$, s^{-2} cm^{-1}	0.1397	0.0911	0.0890
$M_{\delta_{coll}}$, s^{-2} cm^{-1}	0.0450	0.0102	-0.0035
$Z_{\delta_{long}}$, m s^{-2} cm^{-1}	0.0602	-0.1615	-0.1548
$Z_{\delta_{coll}}$, m s^{-2} cm^{-1}	-0.9680	-0.8264	-0.7306
$X_{\delta_{long}}$, m s^{-2} cm^{-1}	0.0119	0.1308	0.1155
$X_{\delta_{coll}}$, m s^{-2} cm^{-1}	0.0663	0.0354	0.0555

TABLE IV.- LATERAL-DIRECTIONAL AERODYNAMIC DERIVATIVES AND TRIM CONDITIONS

Quantity	Derivative model (a)	Run 6	Run 10	Run 18	Run 26	Run 32	Run 40	Run 44
$\bar{U}_o$, knots		0	0	20	40	40	60	60
$\bar{W}_o$, m s^{-1}		0	2.54	2.54	0	2.54	0	2.54
Trim:								
U_o, knots		0.4	1.7	21.8	38.4	47.1	62.8	63.4
W_o, m s^{-1}		-0.00	2.48	3.20	-1.71	2.33	0.85	3.51
Θ_o, deg		8.48	6.72	4.72	4.25	3.08	3.20	0.62
Stability:								
Y_v, s^{-1}	○	-0.1371	-0.1318	-0.1083	-0.0689	-0.0642	-0.0740	-0.0704
Y_v, s^{-1}	□	-0.1170	0.1531	--------	-0.1227	0.1738	0.0271	0.0041
Y_v, s^{-1}	◇	0.0481	--------	--------	0.1872	0.1393	-0.1010	--------
L_v, s^{-1} m^{-1}	○	-0.0200	-0.0191	-0.0185	-0.0182	-0.0171	-0.0180	-0.0168
L_v, s^{-1} m^{-1}	□	-0.0202	-0.0851	--------	-0.0597	-0.1274	0.0316	0.0182
L_v, s^{-1} m^{-1}	◇	0.0216	--------	--------	-0.0239	0.0056	0.0051	--------
L_p, s^{-1}	○	-0.6950	-0.7313	-0.7489	-0.7748	-0.8270	-0.8184	-0.8789
L_p, s^{-1}	□	-1.3592	-1.1532	--------	-0.2166	-0.4264	-0.6662	-0.9739
L_p, s^{-1}	◇	0.4069	--------	--------	0.9993	0.2083	-0.7586	--------
N_v, s^{-1} m^{-1}	○	-0.0020	-0.0018	0.0043	0.0009	0.0007	-0.0003	-0.0005
N_v, s^{-1} m^{-1}	□	-0.0000	0.0076	--------	0.0022	-0.0117	0.0082	-0.0040
N_v, s^{-1} m^{-1}	◇	-0.0158	--------	--------	0.0023	0.0007	-0.0080	--------
N_p, s^{-1}	○	0.0008	-0.0015	-0.0098	-0.0144	-0.0142	-0.0166	-0.0150
N_p, s^{-1}	□	-0.2458	-0.3781	--------	-0.2730	0.4883	0.3367	-0.1738
N_p, s^{-1}	◇	-0.0301	--------	--------	-0.0898	-0.0344	0.0396	--------
N_r, s^{-1}	○	-0.0417	-0.0408	-0.0409	-0.0398	-0.0394	-0.0391	-0.0383
N_r, s^{-1}	□	0.4230	0.3891	--------	0.1842	0.1422	0.1832	1.0857
N_r, s^{-1}	◇	-0.0470	--------	--------	-0.0575	-0.0472	-0.0318	--------
Control:								
$Y_{\delta_{lat}}$, m s^{-2} cm^{-1}	○	0.1391	0.1389	0.1371	0.1352	0.1343	0.1344	0.1331
$Y_{\delta_{lat}}$, m s^{-2} cm^{-1}	□	-0.1736	0.0393	--------	-0.0531	-0.0477	-0.0924	-0.0716
$Y_{\delta_{lat}}$, m s^{-2} cm^{-1}	◇	-0.0818	--------	--------	0.1824	0.1797	0.1210	--------
$Y_{\delta_{rud}}$, m s^{-2} cm^{-1}	○	-0.0065	-0.0066	-0.0045	-0.0046	-0.0050	-0.0064	-0.0072
$Y_{\delta_{rud}}$, m s^{-2} cm^{-1}	□	[b](-0.0065)	[b](-0.0066)	--------	0.1089	0.0792	0.0642	0.0509
$Y_{\delta_{rud}}$, m s^{-2} cm^{-1}	◇	-0.0059	--------	--------	-0.0036	-0.0049	-0.0063	--------
$L_{\delta_{lat}}$, s^{-2} cm^{-1}	○	0.1636	0.1634	0.1617	0.1601	0.1594	0.1597	0.1587
$L_{\delta_{lat}}$, s^{-2} cm^{-1}	□	0.2030	0.1303	--------	0.1777	0.1772	0.2367	0.2065
$L_{\delta_{lat}}$, s^{-2} cm^{-1}	◇	0.1637	--------	--------	0.2402	0.1635	0.0522	--------
$L_{\delta_{rud}}$, s^{-2} cm^{-1}	○	-0.0547	-0.0547	-0.0523	-0.0518	-0.0518	-0.0530	-0.0532
$L_{\delta_{rud}}$, s^{-2} cm^{-1}	□	[b](-0.0547)	[b](-0.0547)	--------	-0.0558	-0.0416	-0.0489	-0.1020
$L_{\delta_{rud}}$, s^{-2} cm^{-1}	◇	-0.0155	--------	--------	-0.0667	-0.1403	-0.0501	--------
$N_{\delta_{lat}}$, s^{-2} cm^{-1}	○	0.0036	0.0036	0.0040	0.0039	0.0038	0.0035	0.0033
$N_{\delta_{lat}}$, s^{-2} cm^{-1}	□	0.0204	0.0318	--------	0.0121	0.0129	-0.0360	0.0128
$N_{\delta_{lat}}$, s^{-2} cm^{-1}	◇	-0.0068	--------	--------	-0.0036	0.0052	-0.0007	--------
$N_{\delta_{rud}}$, s^{-2} cm^{-1}	○	0.0802	0.0801	0.0792	0.0780	0.0775	0.0776	0.0768
$N_{\delta_{rud}}$, s^{-2} cm^{-1}	□	[b](0.0802)	[b](0.0801)	--------	0.0609	0.0433	0.0228	0.0681
$N_{\delta_{rud}}$, s^{-2} cm^{-1}	◇	0.0211	--------	--------	0.0312	0.0490	0.0291	--------

[a]○ Reference 2 □ MLE ◇ EKF (ref. 4).
[b]Held constant at reference 2 values.

TABLE V.- CH-47 FLIGHT TEST RUN SCHEDULE

(a) Single input maneuvers

Test point	Run	Control input	Airspeed $\bar{U}_o$, knots	Descent rate $\bar{W}_o$, m/sec	Wind velocity, knots	Altitude, m
Computer generated						
2	5 6 7 8	δ_{long} δ_{lat} δ_{rud} δ_{coll}	0 (Hover)	0	3	61.0
3	9 10 11 12	δ_{long} δ_{lat} δ_{rud} δ_{coll}	0	2.54	3	137.2
4	13 14 15 16	δ_{long} δ_{lat} δ_{rud} δ_{coll}	0 (Hover)	0	4	15.2 (In ground effect)
5	17 18 19 20	δ_{long} δ_{lat} δ_{rud} δ_{coll}	20	2.54	7	259.1
Manual						
1	1 2 3 4	δ_{long} δ_{lat} δ_{rud} δ_{coll}	0 (Hover)	0	3	61.0
6	21 22 23 24	δ_{long} δ_{lat} δ_{rud} δ_{coll}	40	0	13	243.8
12	35 36 37 38	δ_{long} δ_{lat} δ_{rud} δ_{coll}	60	0	20	243.8

TABLE V.- Concluded

(b) Computer-generated double input maneuvers

Test point	Run	Control input	Airspeed $\bar{U}_o$, knots	Descent rate $\bar{W}_o$, m/sec	Wind velocity, knots	Altitude, m
7	25 26	δ_{long}; δ_{coll} δ_{lat}; δ_{rud}	40	0	13 10	243.8
8	27 28	δ_{long}; δ_{coll} δ_{lat}; δ_{rud}	40	-5.08	8 7	213.4
9	29 30	δ_{long}; δ_{coll} δ_{lat}; δ_{rud}	40	-2.54	8 8	228.6
10	31 32	δ_{long}; δ_{coll} δ_{lat}; δ_{rud}	40	2.54	11 11	259.1
11	33 34	δ_{long}; δ_{coll} δ_{lat}; δ_{rud}	40	5.08	11 8	274.3
13	39 40	δ_{long}; δ_{coll} δ_{lat}; δ_{rud}	60	0	20 20	243.8
14	41 42	δ_{long}; δ_{coll} δ_{lat}; δ_{rud}	60	2.54	6 6	259.1
15	43 44	δ_{long}; δ_{coll} δ_{lat}; δ_{rud}	60	2.54	20 8	259.1

TABLE VI.- COEFFICIENTS FOR COMPUTER-GENERATED INPUTS

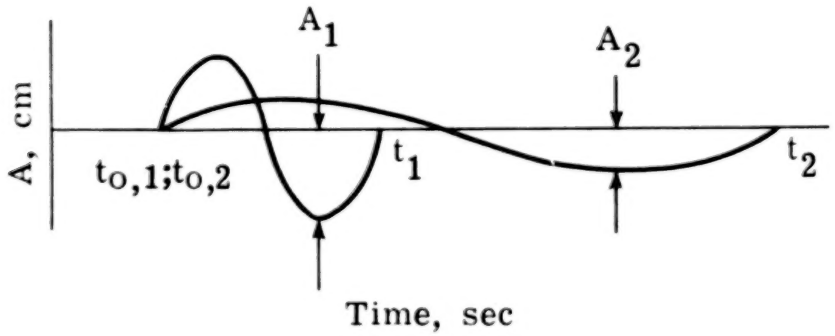

u	A_1, cm	A_2, cm	ω_1, rad/sec	ω_2, rad/sec	$t_{o,1}$, sec	$t_{o,2}$, sec	t_1, sec	t_2, sec
Single input maneuvers at hover and 20 knots								
[a]δ_{long}	5.08	1.27	3.43	0.53	0	0	1.83	12
[a]δ_{coll}	3.81	1.27	3.43	.53	0	0	1.83	12
δ_{lat}	3.81	.25	2.70	.32	0	0	2.33	>15
δ_{rud}	3.56	.51	2.70	.32	0	0	2.33	>15
Double input maneuvers at 40 and 60 knots								
δ_{long}	3.56	0.89	3.43	0.53	0	6	1.8	12
δ_{coll}	3.56	.89	3.43	.53	6	6	7.8	12
δ_{lat}	2.54	.25	3.50	.32	0	0	1.8	>15
δ_{rud}	-2.54	-.25	3.50	.32	6	6	7.8	>15

[a]Longitudinal inputs were implemented with opposite signs in flight test because of sign convention employed in reference 3.

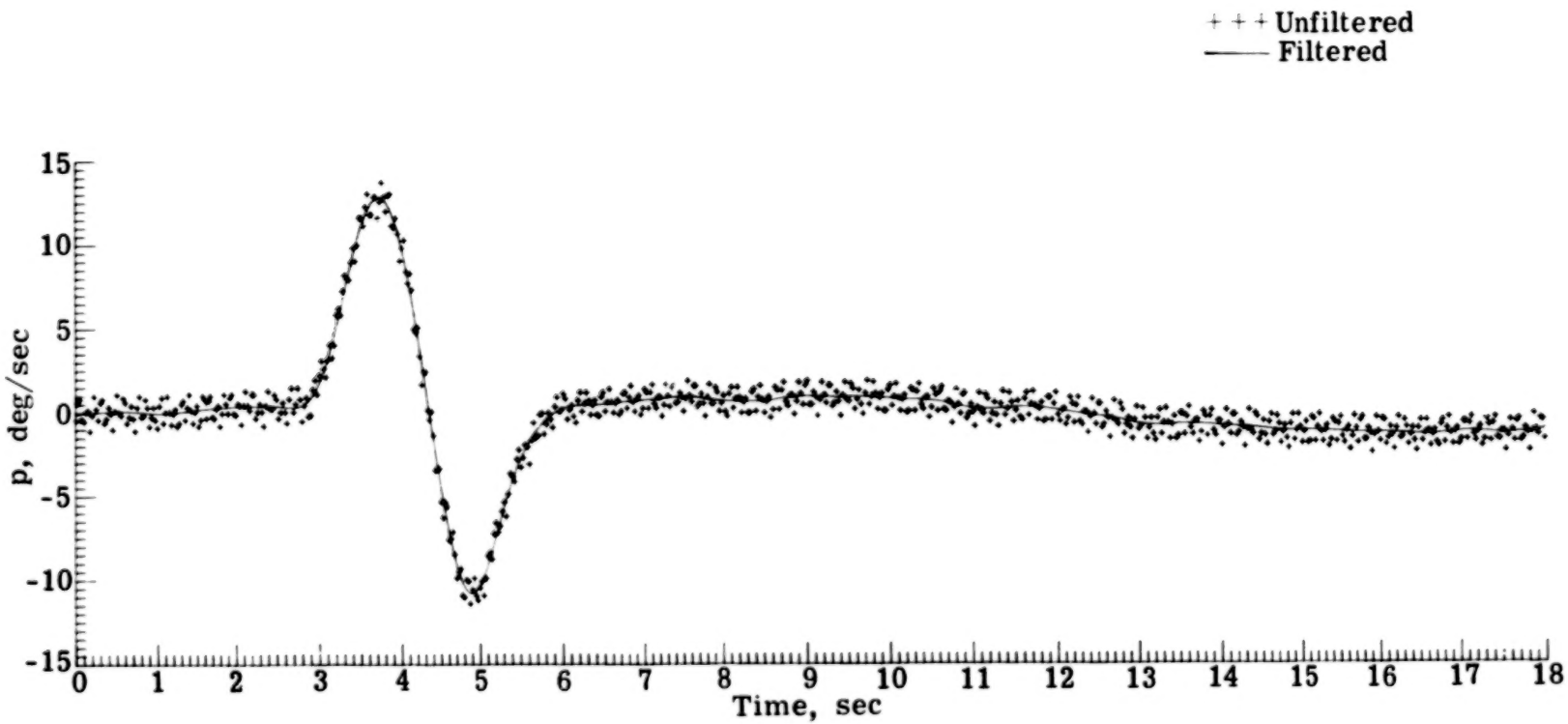

Figure 1.- Digital filtering of flight data from run 10.

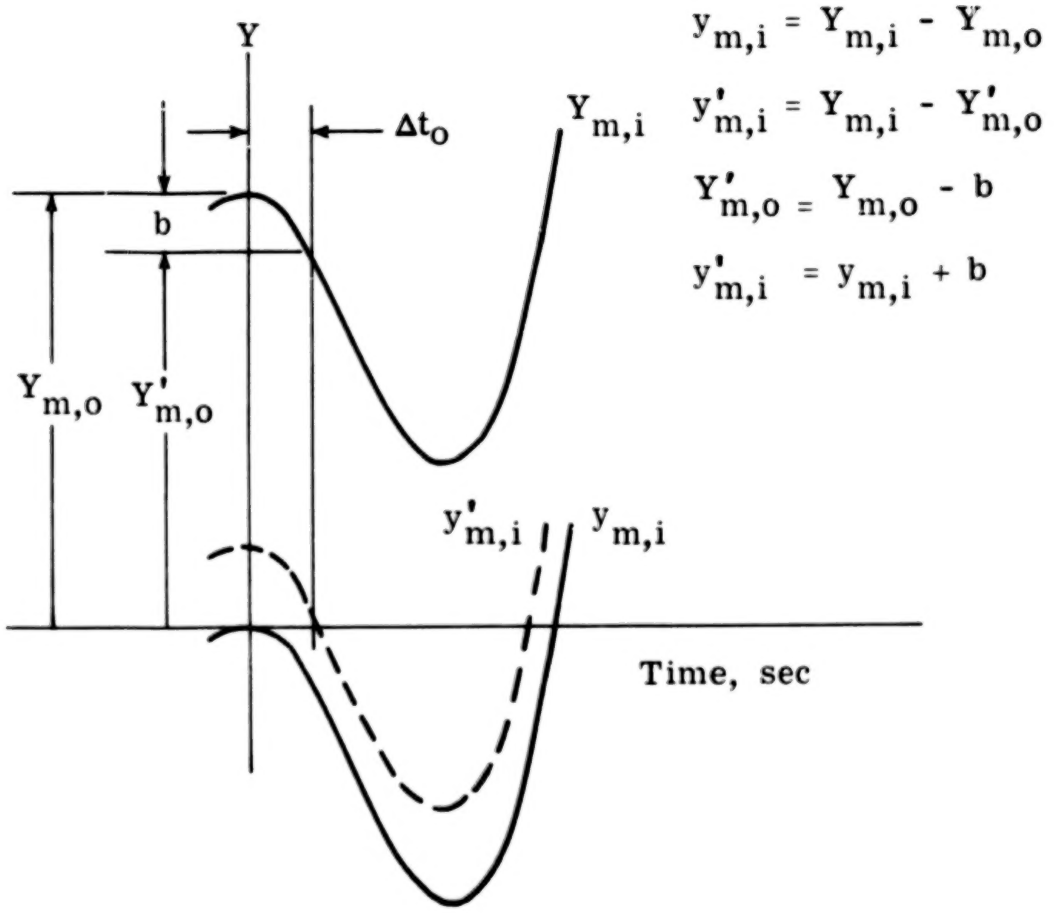

Figure 2.- Reduction of flight data to perturbation format.

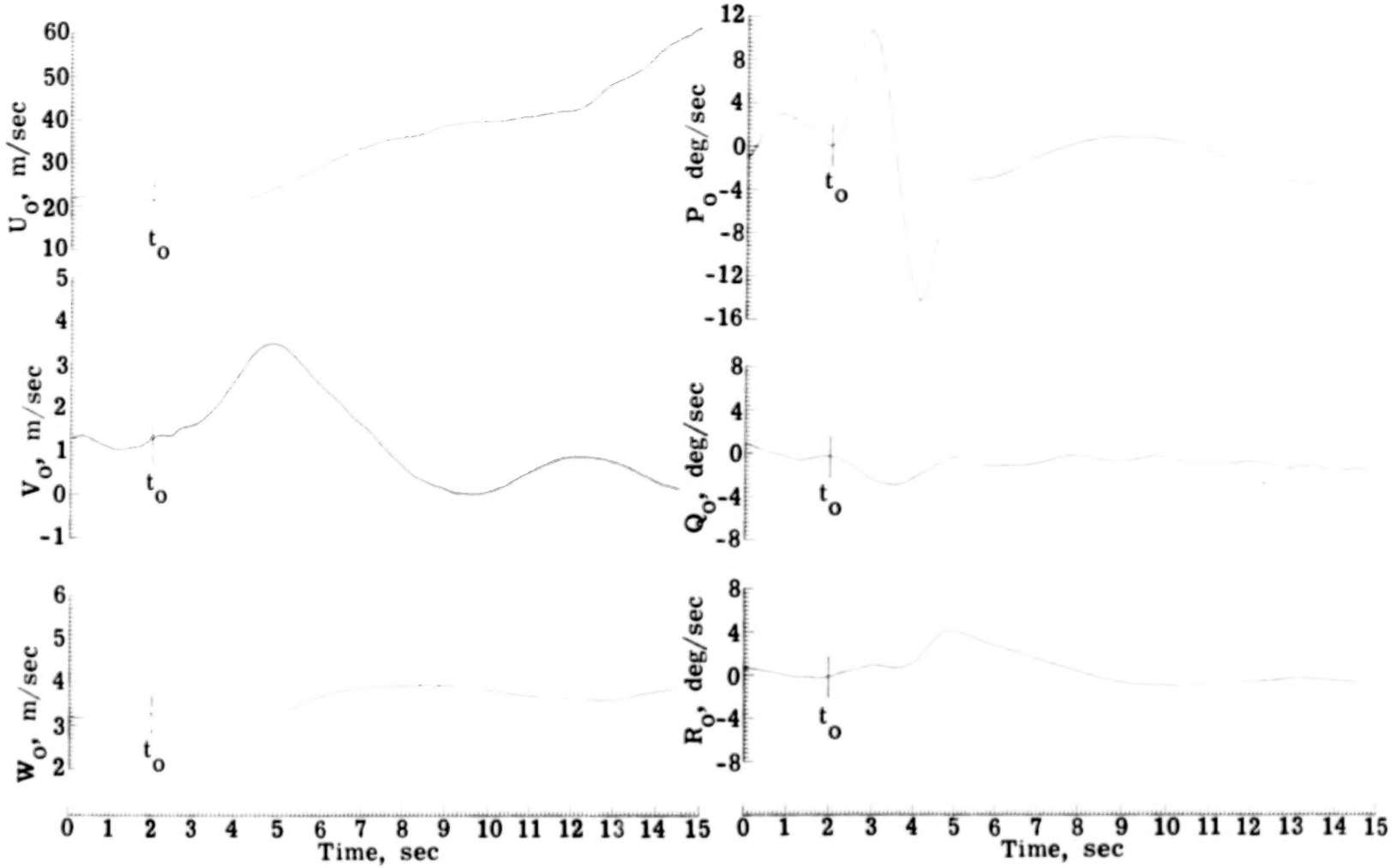

Figure 3.- Typical trim conditions. Run 18; $\bar{U}_o$ = 20 knots; $\bar{W}_o$ = 2.54 m/sec.

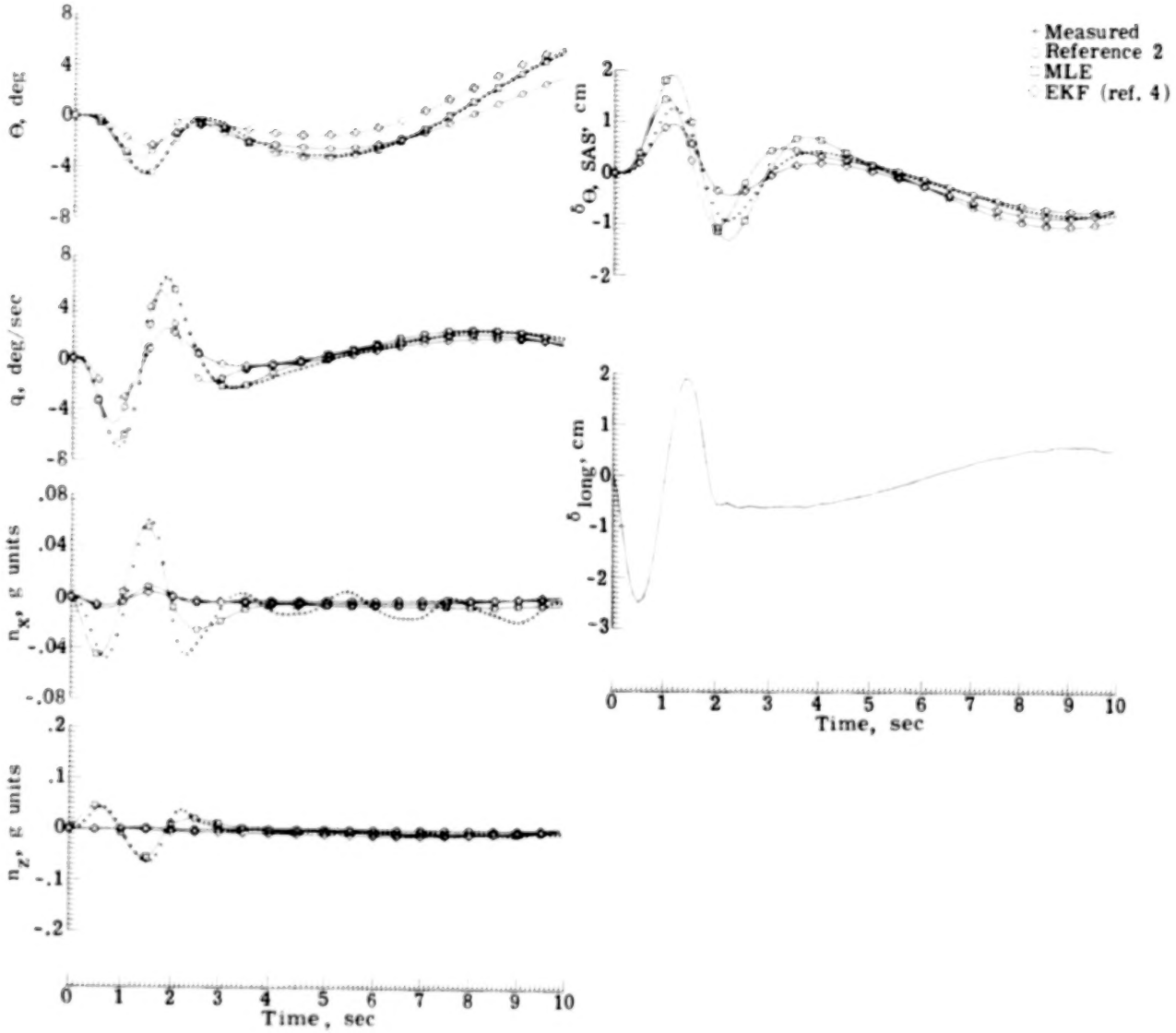

(a) Run 5; $\bar{U}_o = 0$; $\bar{W}_o = 0$.

Figure 4.- Comparison of longitudinal response time histories.

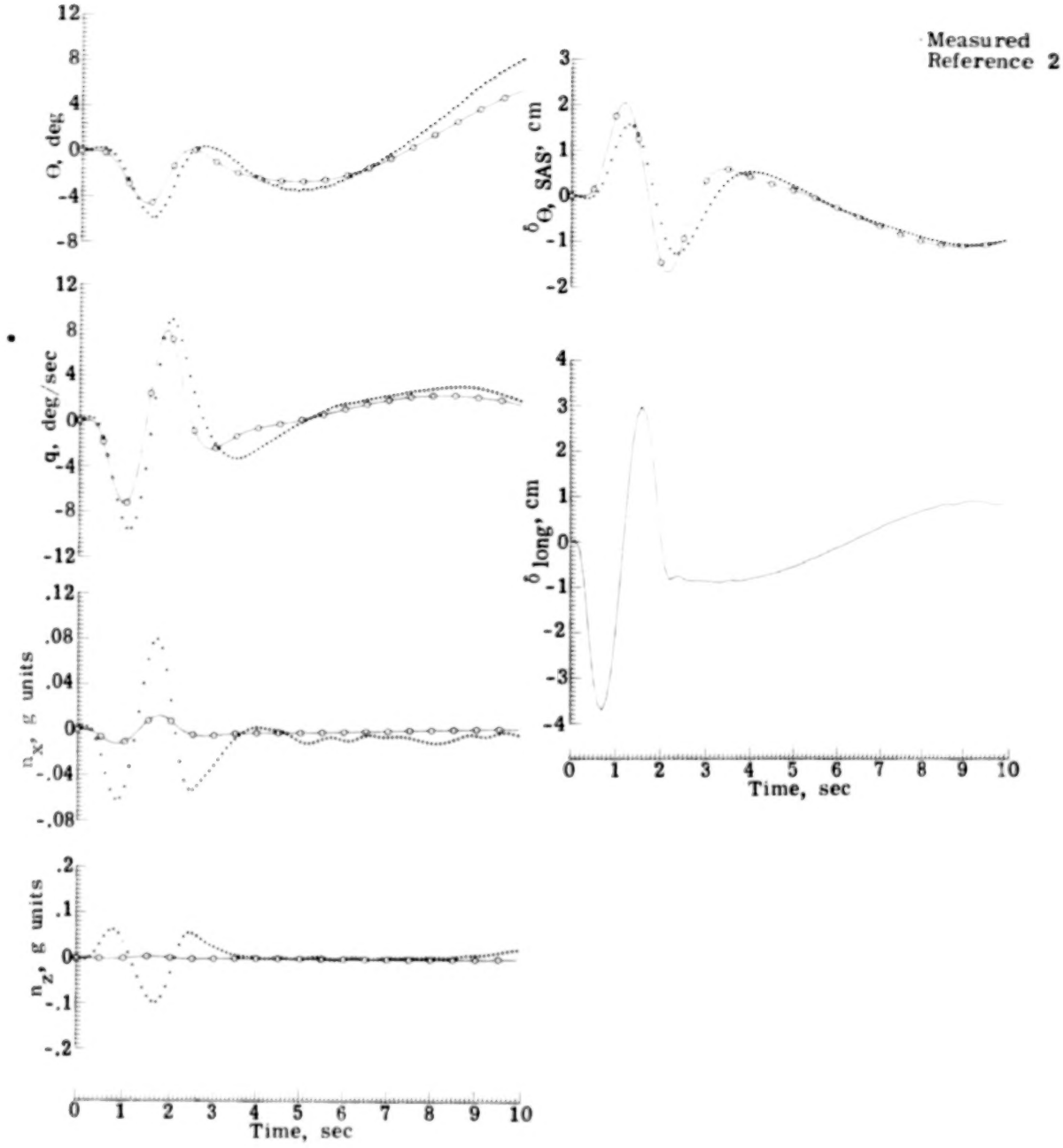

(b) Run 9; $\bar{U}_o = 0$; $\bar{W}_o = 2.54$ m/sec.

Figure 4.- Continued.

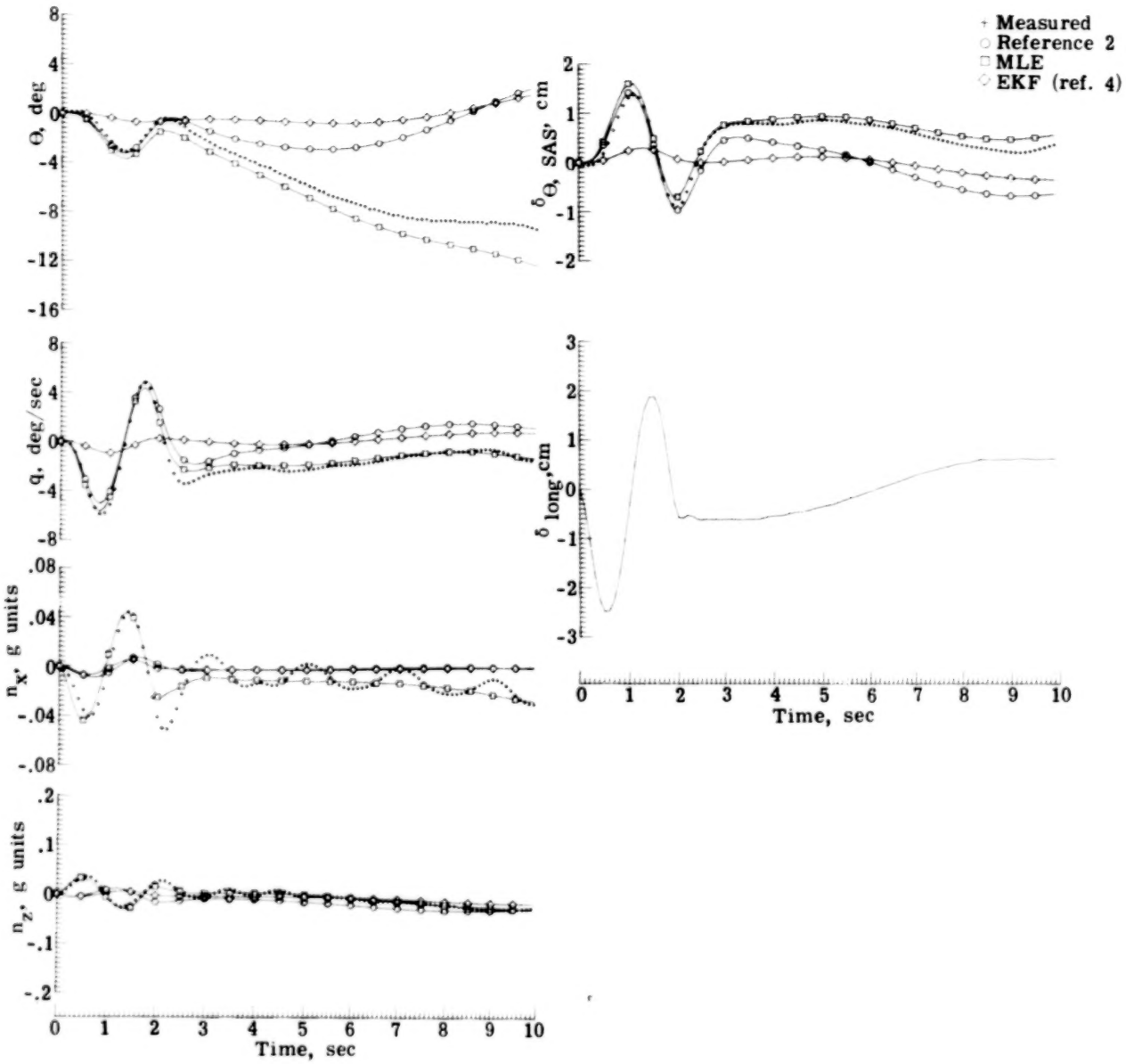

(c) Run 17; $\bar{U}_o$ = 20 knots; $\bar{W}_o$ = 2.54 m/sec.

Figure 4.- Continued.

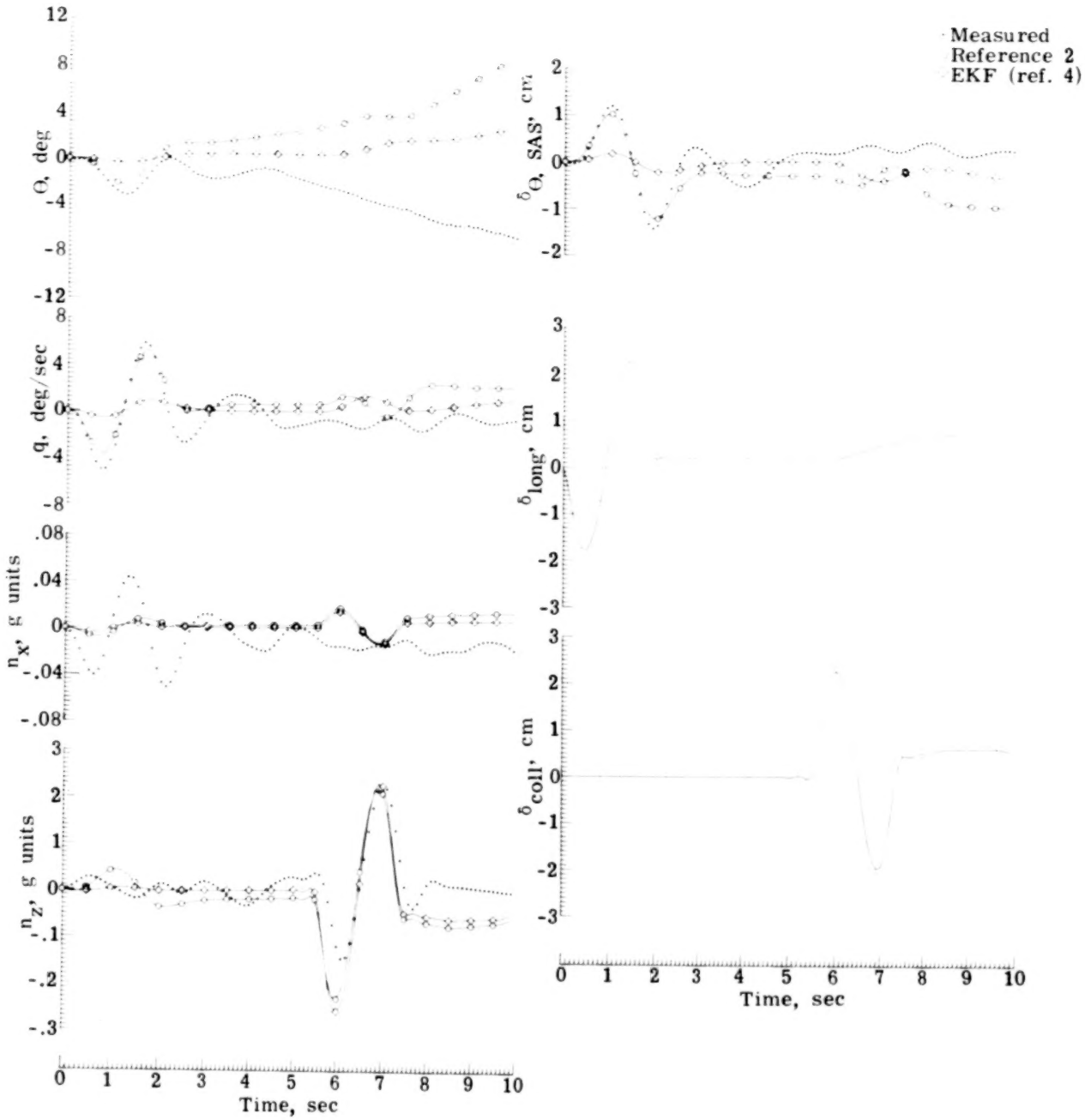

(d) Run 25; $\bar{U}_o$ = 40 knots; $\bar{W}_o$ = 0.

Figure 4.- Continued.

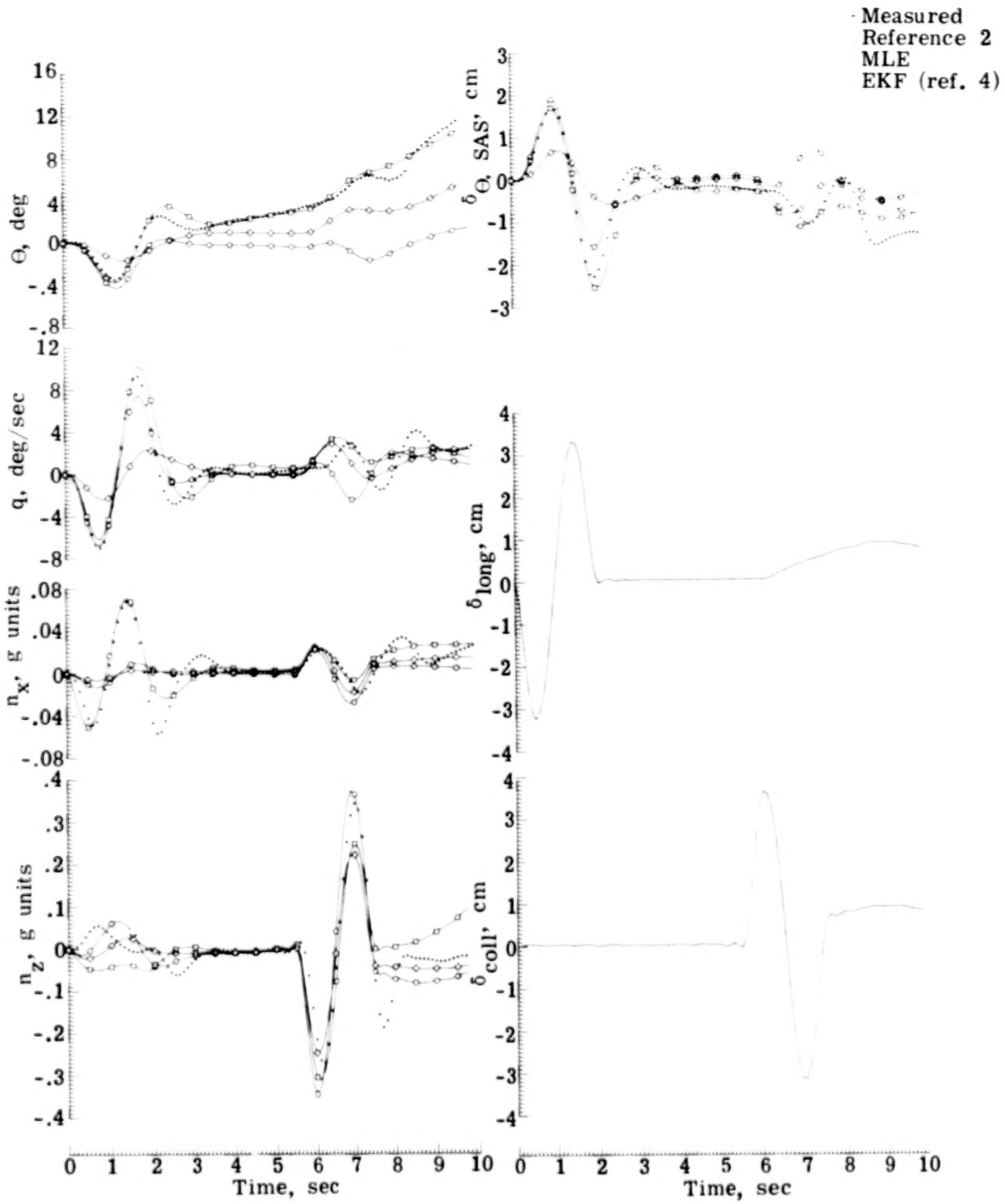

(e) Run 31; $\bar{U}_o$ = 40 knots; $\bar{W}_o$ = 2.54 m/sec.

Figure 4.- Continued.

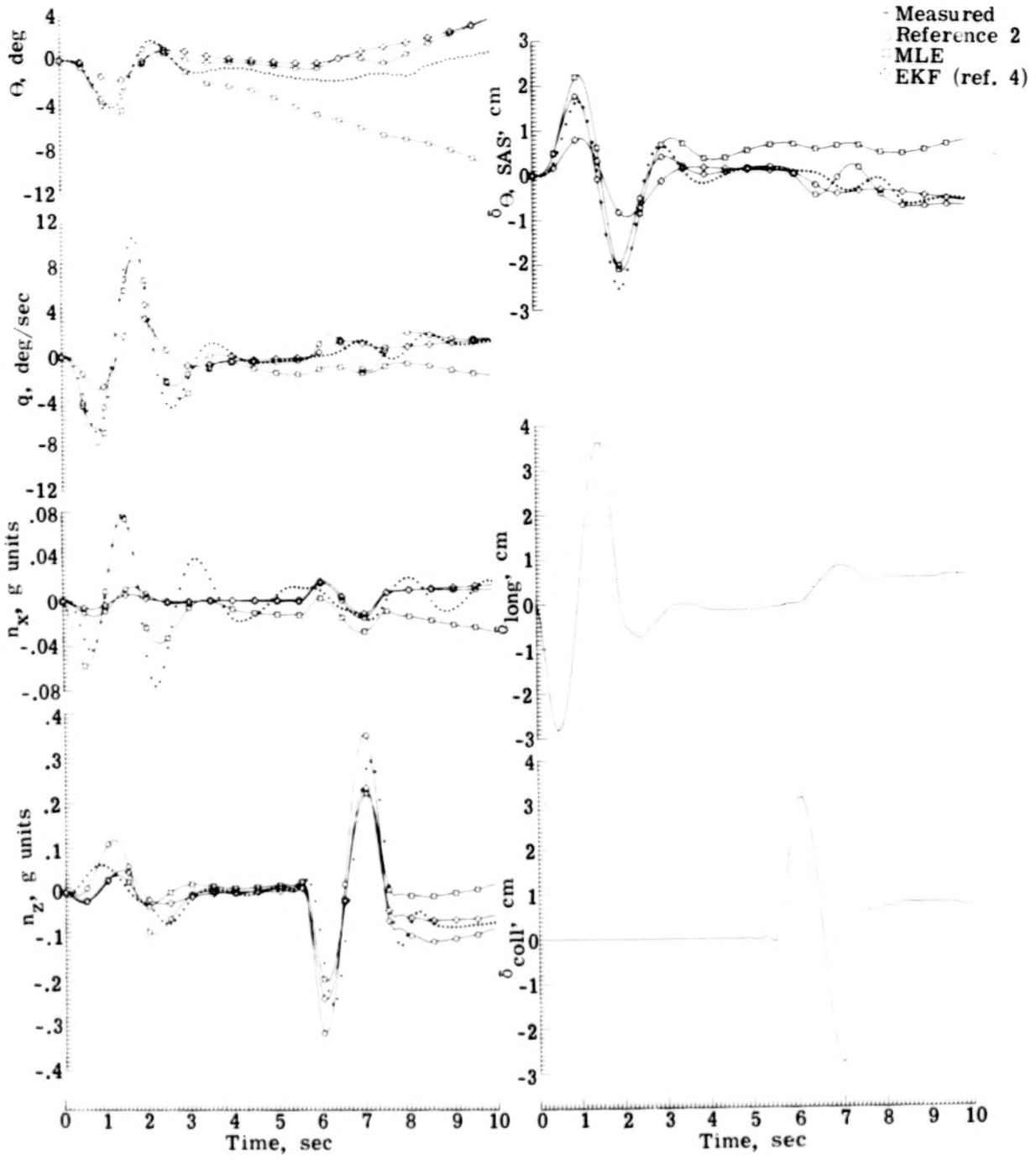

(f) Run 39; $\bar{U}_o$ = 60 knots; $\bar{W}_o$ = 0.

Figure 4.- Continued.

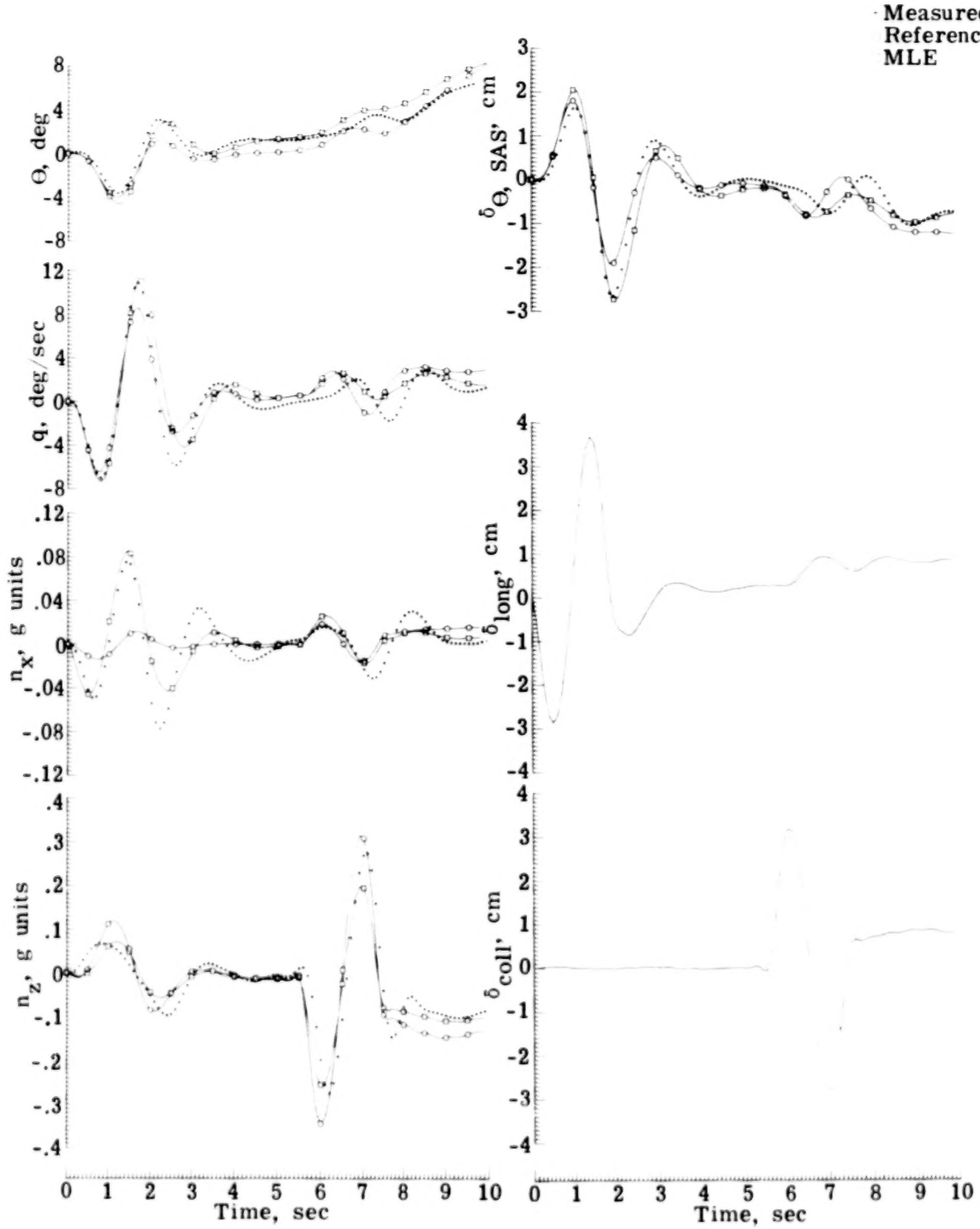

(g) Run 43; $\bar{U}_o$ = 60 knots; $\bar{W}_o$ = 2.54 m/sec.

Figure 4.- Concluded.

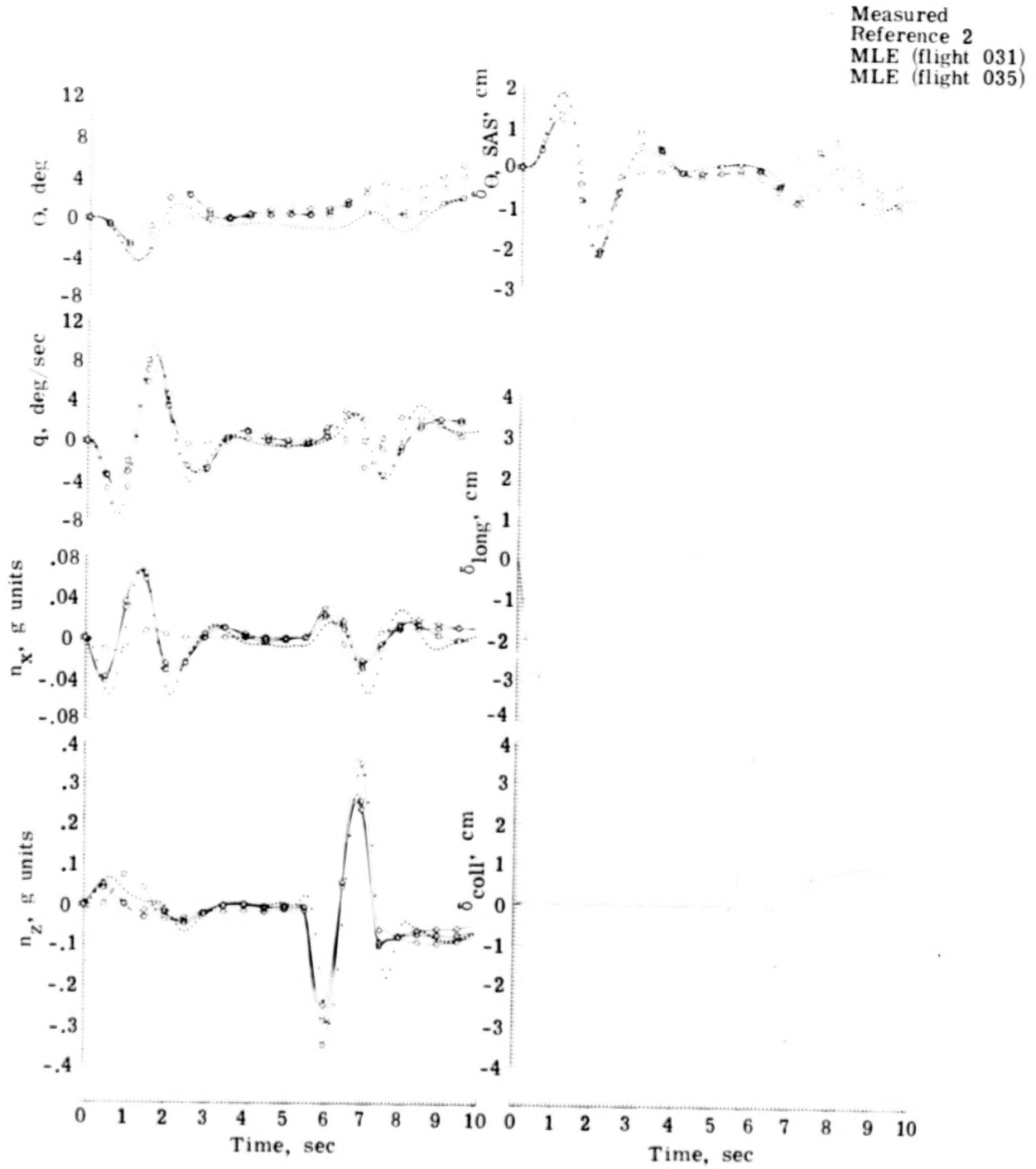

(a) Run 33 (flight 031); $\bar{U}_o$ = 40 knots; $\bar{W}_o$ = 5.08 m/sec.

Figure 5.- Comparison of longitudinal response time histories for two different flights at same test conditions.

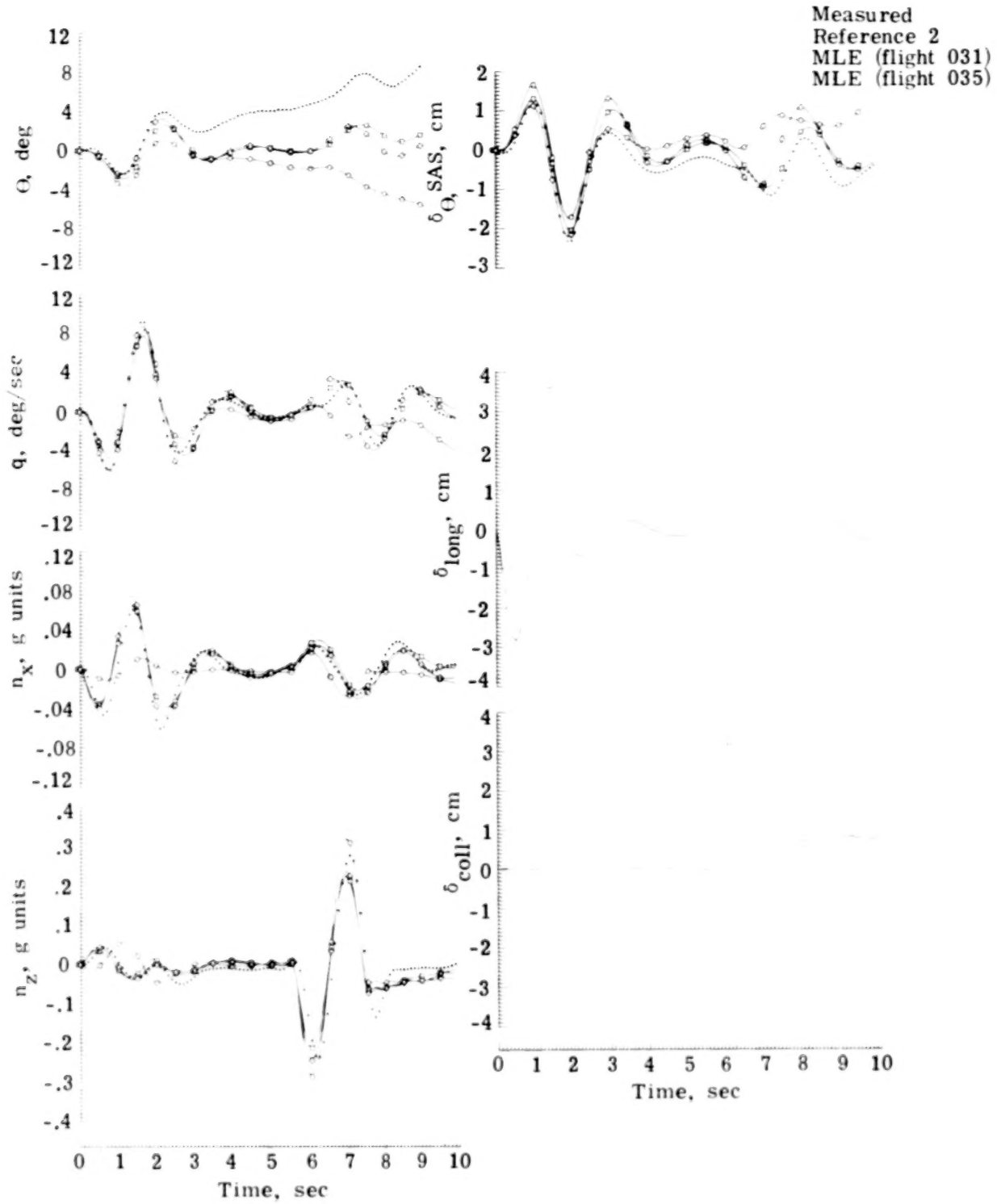

(b) Run 33 (flight 035); $\bar{U}_o$ = 40 knots; $\bar{W}_o$ = 5.08 m/sec.

Figure 5.- Concluded.

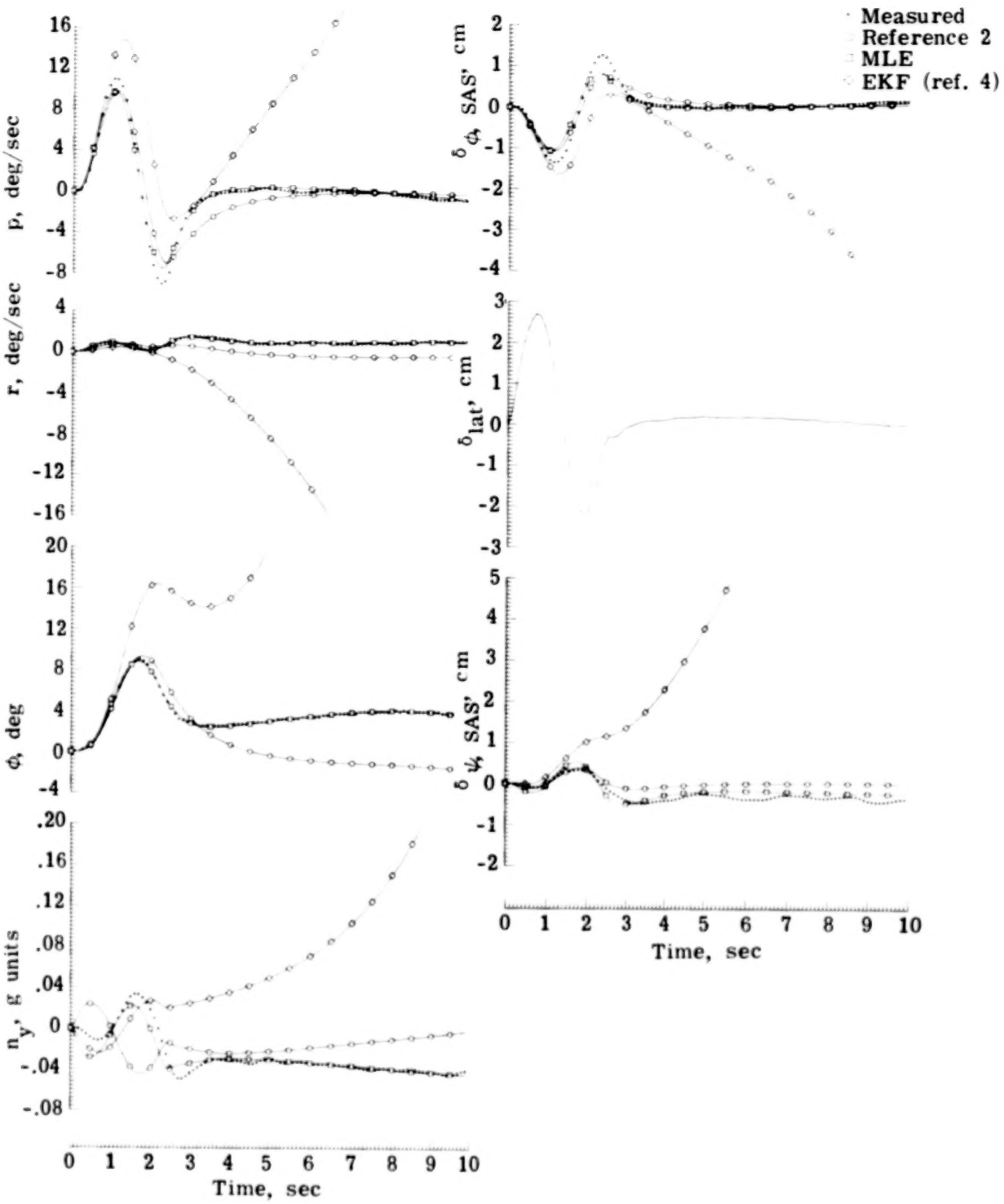

(a) Run 6; $\bar{U}_o = 0$; $\bar{W}_o = 0$.

Figure 6.- Comparison of lateral-directional response time histories.

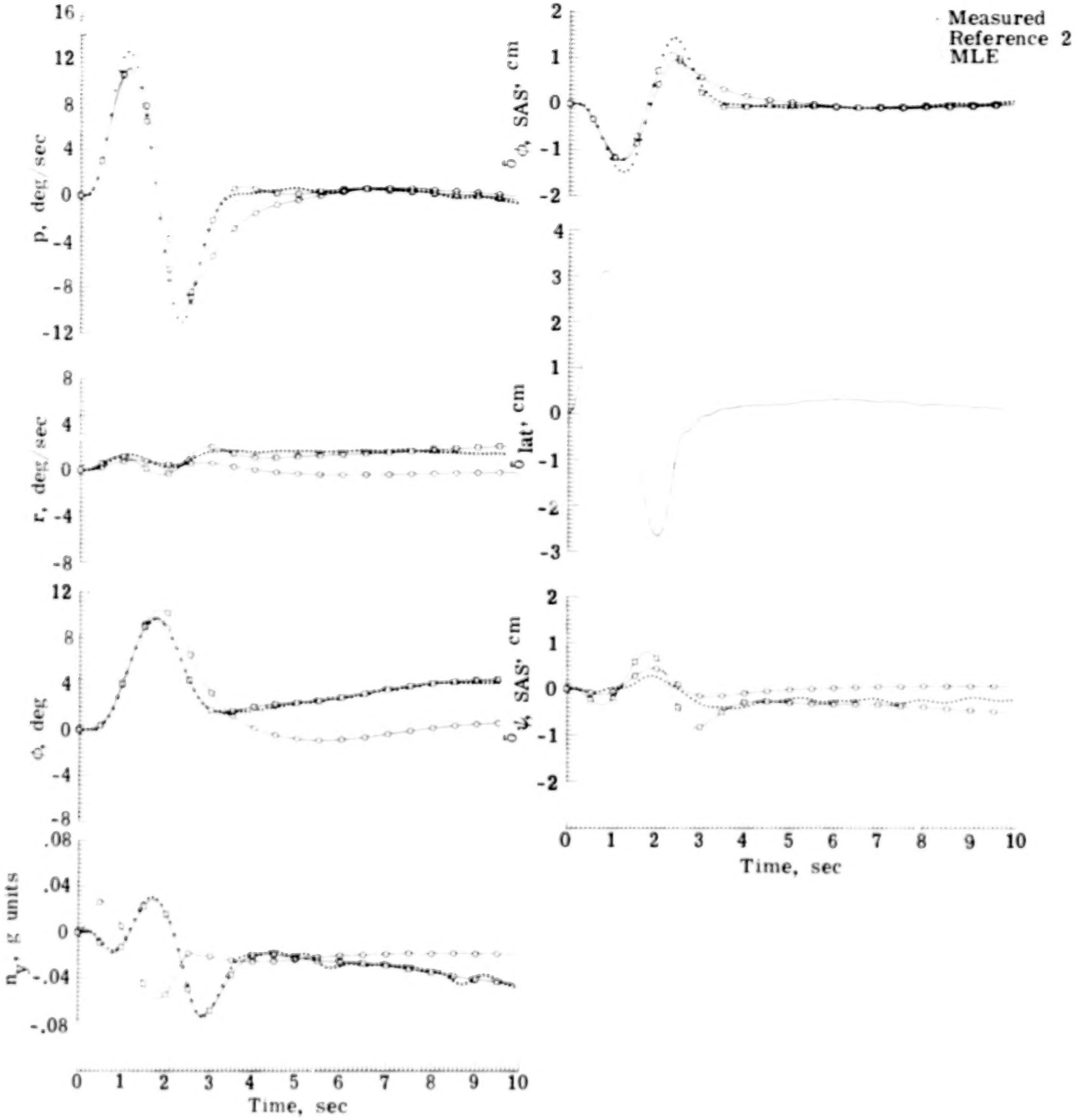

(b) Run 10; $\bar{U}_o = 0$; $\bar{W}_o = 2.54$ m/sec.

Figure 6.- Continued.

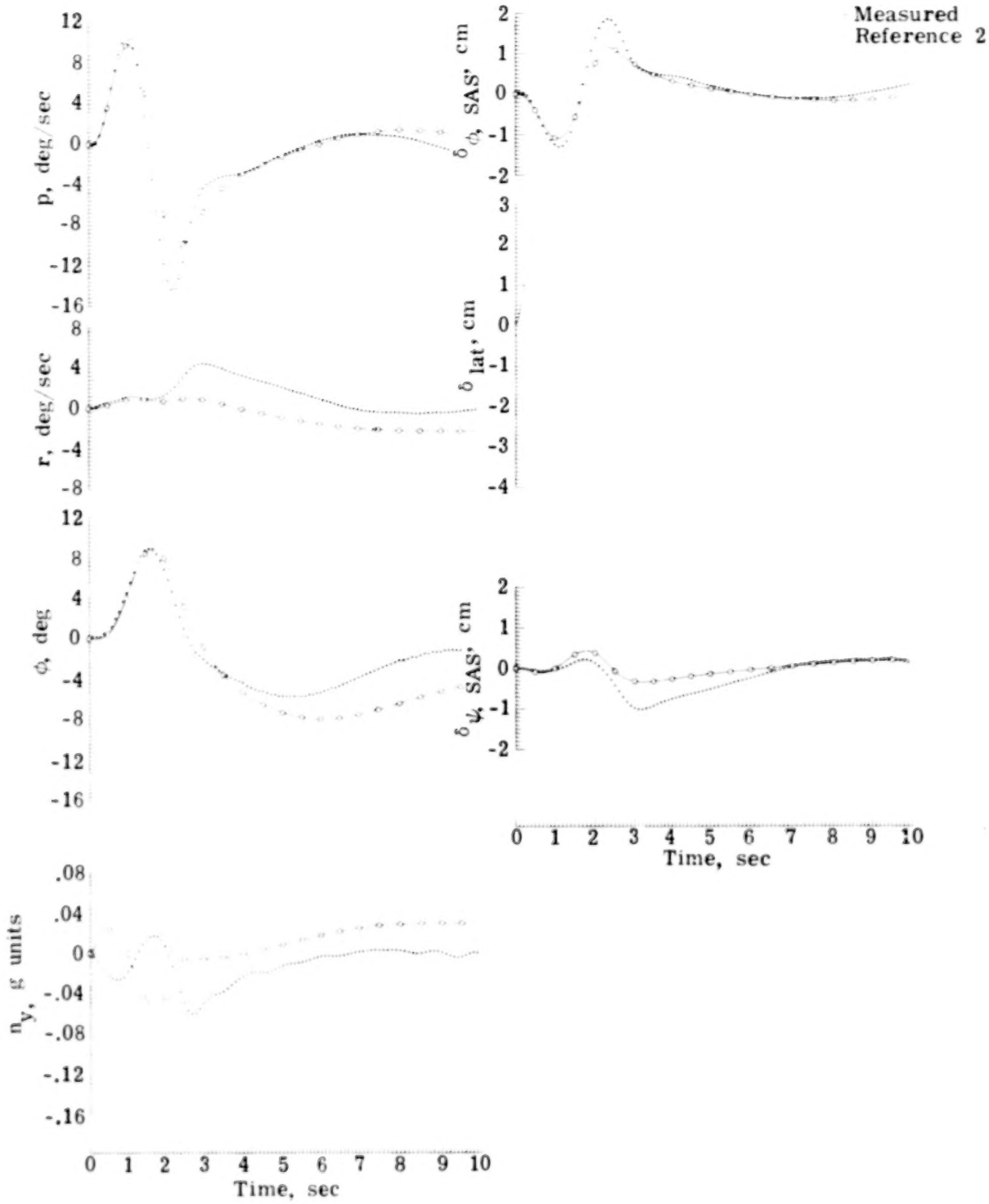

(c) Run 18; $\bar{U}_o$ = 20 knots; $\bar{W}_o$ = 2.54 m/sec.

Figure 6.- Continued.

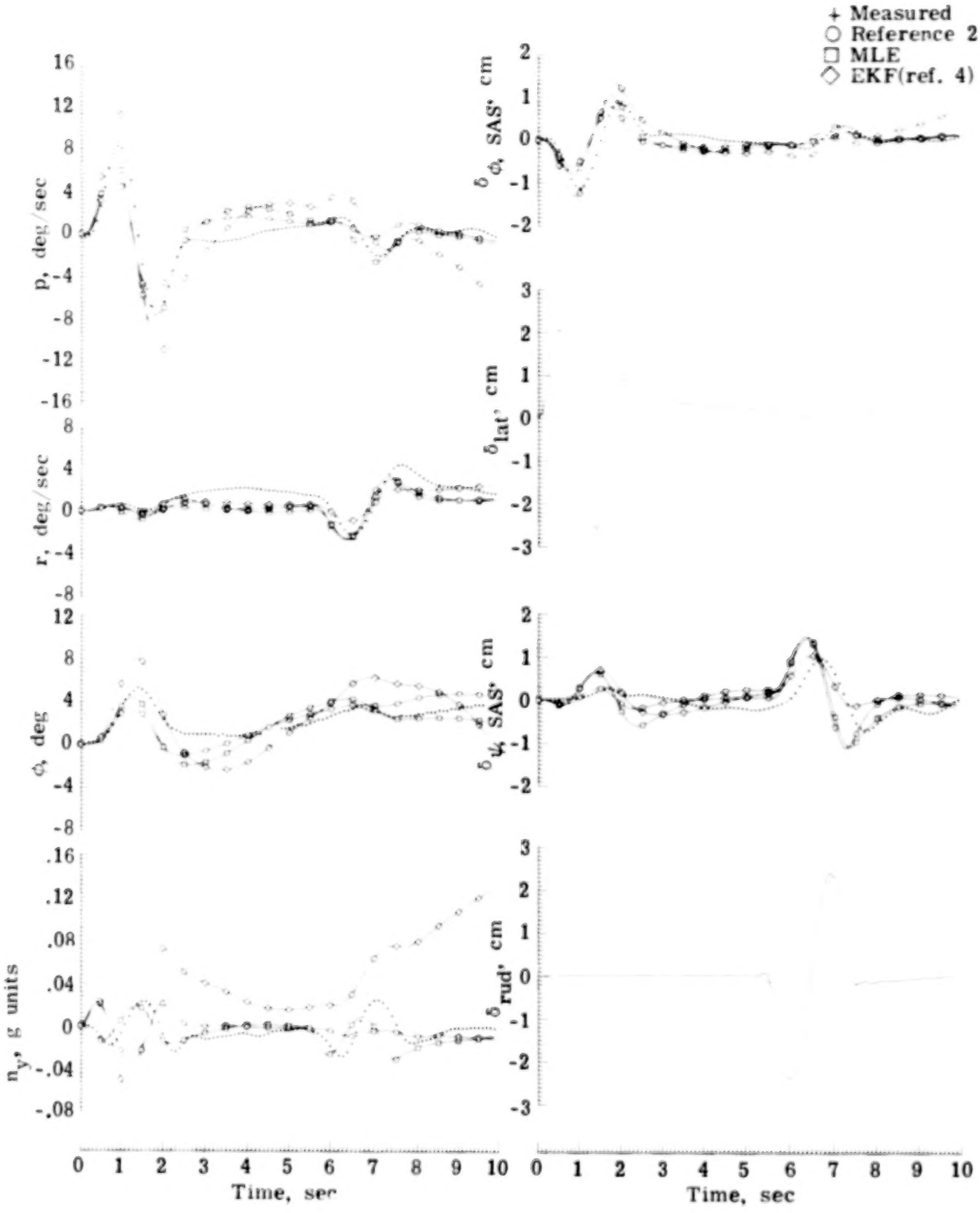

(d) Run 26; $\bar{U}_o$ = 40 knots; $\bar{W}_o$ = 0.

Figure 6.- Continued.

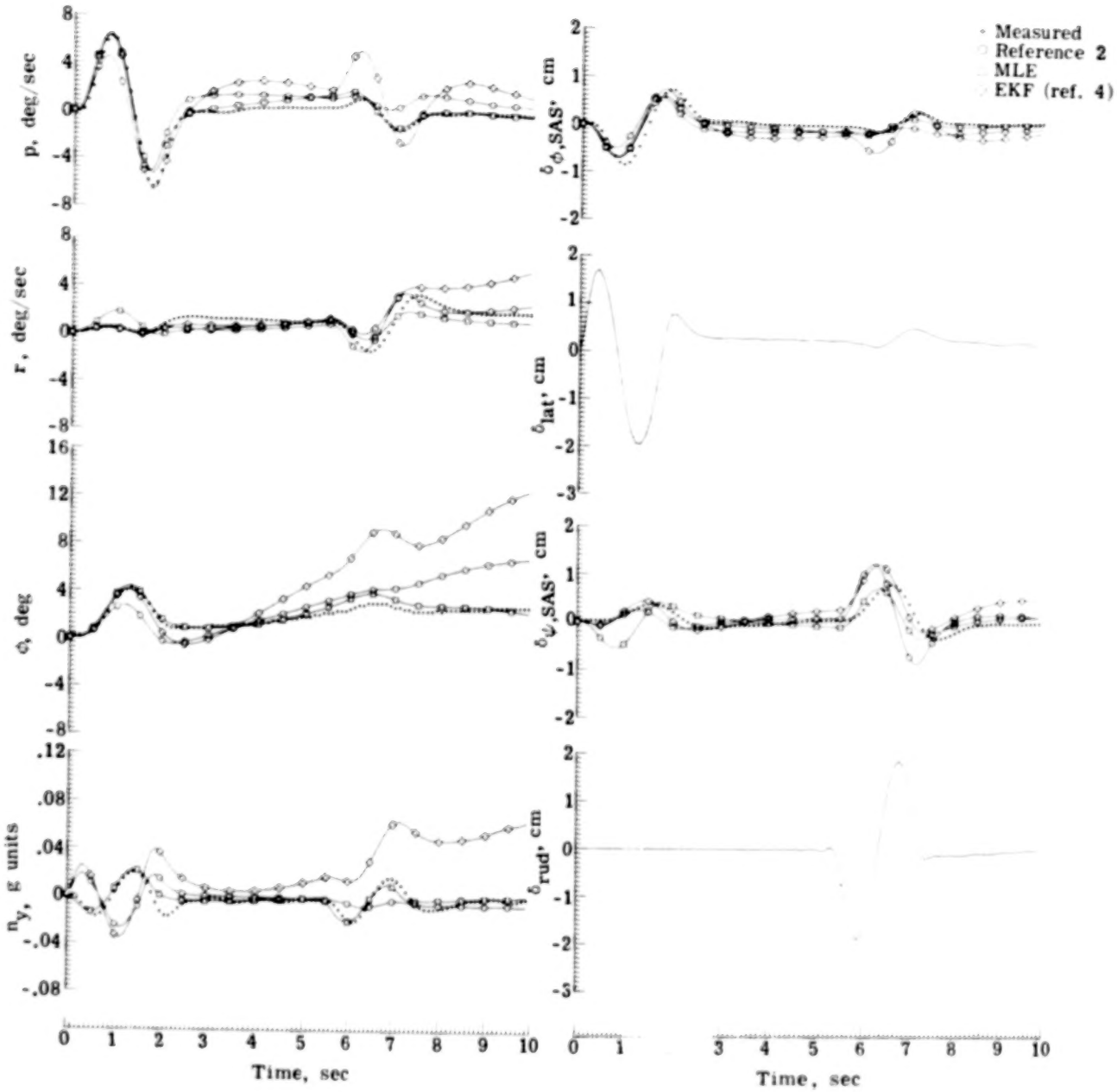

(e) Run 32; $\bar{U}_o$ = 40 knots; $\bar{W}_o$ = 2.54 m/sec.

Figure 6.- Continued.

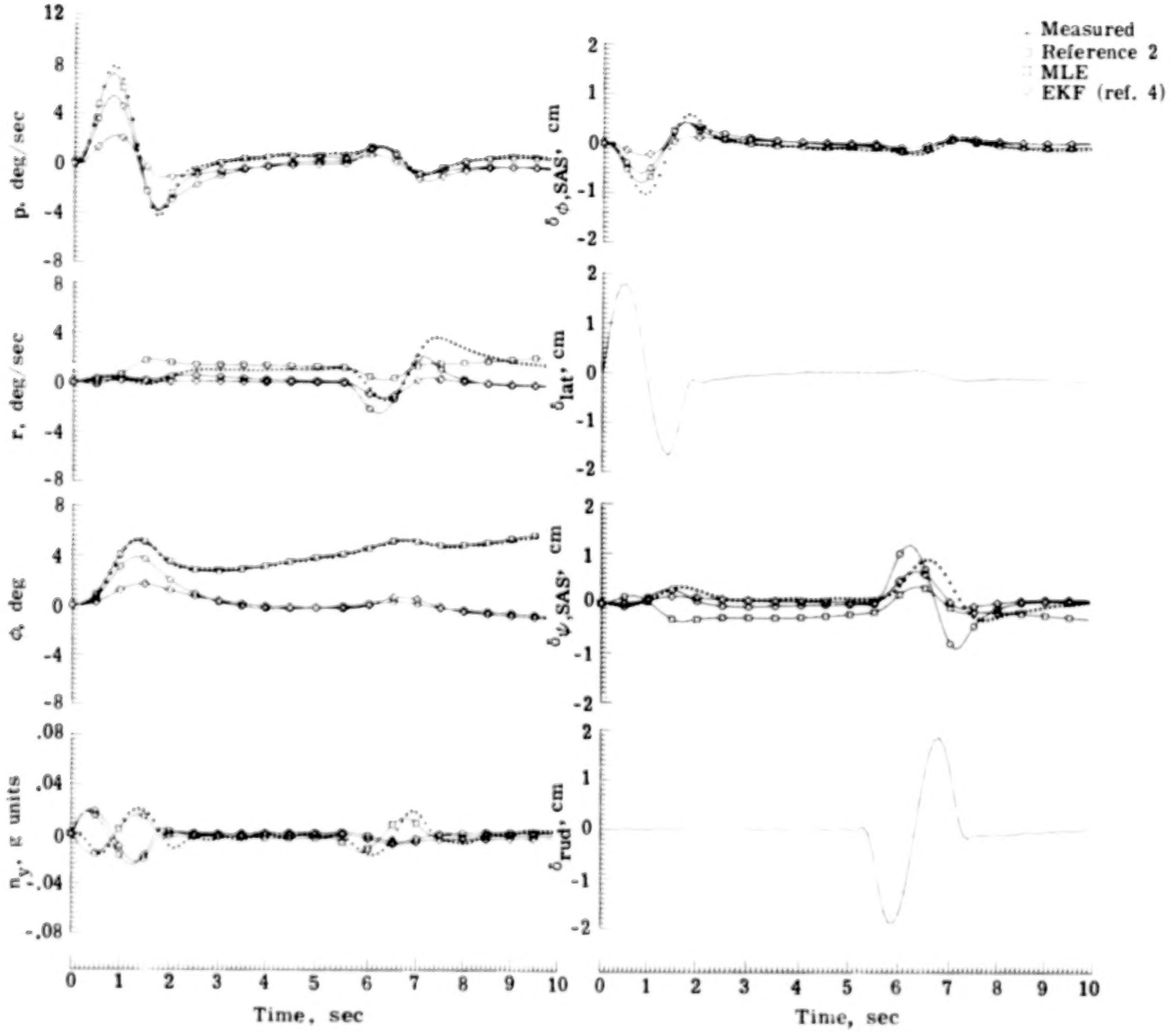

(f) Run 40; $\bar{U}_o$ = 60 knots; $\bar{W}_o$ = 0.

Figure 6.- Continued.

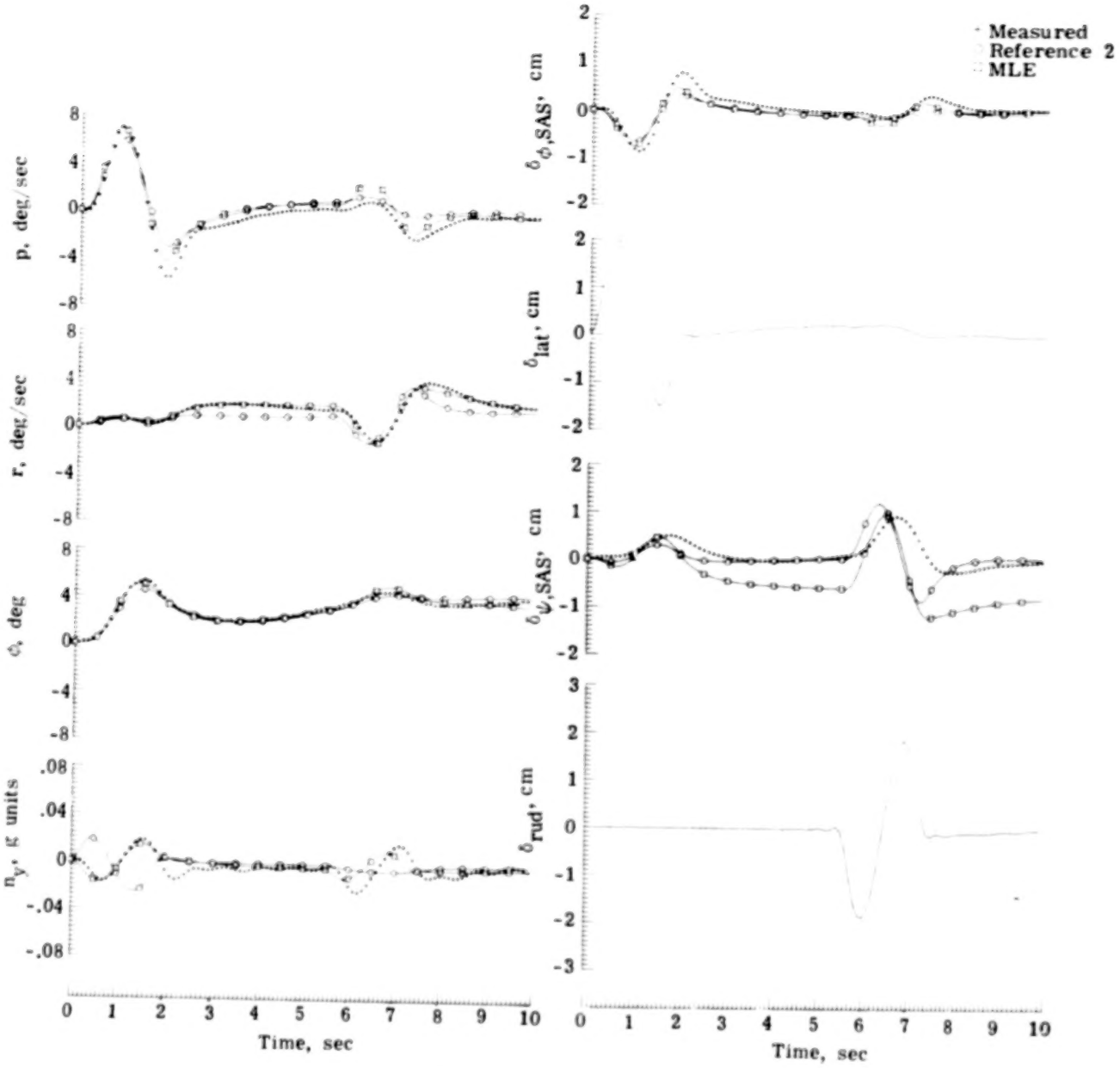

(g) Run 44; $\bar{U}_o$ = 60 knots; $\bar{W}_o$ = 2.54 m/sec.

Figure 6.- Concluded.

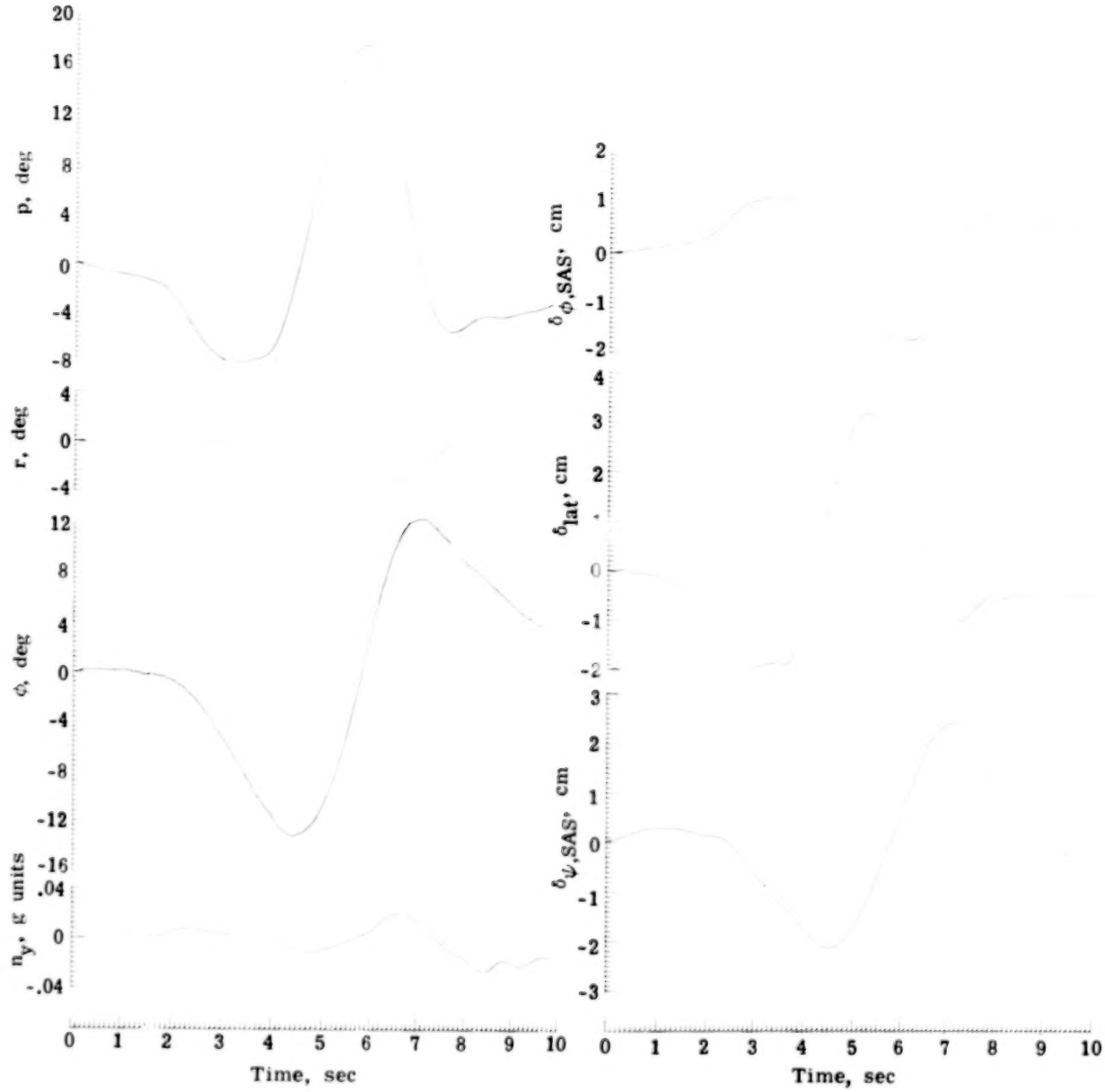

Figure 7.- Typical lateral-directional response time histories generated by manual input maneuver. Run 36; $\bar{U}_o$ = 40 knots; $\bar{W}_o$ = 0.

1. Report No.	2. Government Accession No.	3. Recipient's Catalog No.
NASA TP-1581		

4. Title and Subtitle	5. Report Date
COMPARISON OF ANALYTICAL AND FLIGHT TEST IDENTIFIED AERODYNAMIC DERIVATIVES FOR A TANDEM-ROTOR TRANSPORT HELICOPTER	February 1980
	6. Performing Organization Code
7. Author(s)	8. Performing Organization Report No.
Ward F. Hodge	L-13228
	10. Work Unit No.
9. Performing Organization Name and Address	505-34-33-01
NASA Langley Research Center Hampton, VA 23665	11. Contract or Grant No.
	13. Type of Report and Period Covered
12. Sponsoring Agency Name and Address	Technical Publication
National Aeronautics and Space Administration Washington, DC 20546	14. Sponsoring Agency Code

15. Supplementary Notes

16. Abstract

Flight tests for verifying an analytical aerodynamic derivative model of a CH-47 helicopter were conducted for low cruise speeds and transition to hover portions of curved, decelerating landing approach trajectories. All testing was performed on a closed loop basis with the stability augmentation system of the helicopter operating, and response data were obtained using both manual and computer-generated input maneuvers. The results indicate some differences between the measured response time histories and those predicted by both analytical and flight test identified derivatives. With some exceptions the discrepancies are not severe, and the overall agreement between the measured and computed time histories is reasonably good. No adverse effects attributable to closed loop testing were noted, and the use of computer-generated inputs proved to be superior to manual ones.

17. Key Words (Suggested by Author(s))

Stability and control derivatives
Parameter identification
VALT program
Tandem-rotor helicopters
Derivative identification flight tests
Systems identification

18. Distribution Statement

Unclassified - Unlimited

Subject Category 05

19. Security Classif. (of this report)	20. Security Classif. (of this page)	21. No. of Pages	22. Price*
Unclassified	Unclassified	53	$5.25

* For sale by the National Technical Information Service, Springfield, Virginia 22161

NASA-Langley, 1980